COMPLIANT FOOT SYSTEM DESIGN FOR BIPEDAL ROBOT

TAN BOON HWA

NATIONAL UNIVERSITY OF SINGAPORE

2013

COMPLIANT FOOT SYSTEM DESIGN FOR BIPEDAL ROBOT

TAN BOON HWA

B.Eng. (Hons.), NUS

A THESIS SUBMITTED

FOR THE DEGREE OF MASTER OF ENGINEERING

DEPARTMENT OF MECHANICAL ENGINEERING

NATIONAL UNIVERSITY OF SINGAPORE

2013

DECLARATION

I hereby declare that the thesis is my original work and it has been written by me in its entirety. I have duly acknowledged all the sources of information which have been used in the thesis.

This thesis has also not been submitted for any degree in any university previously.

Tan Boon Hwa
12 August 2013

Acknowledgment

The author wishes to express his sincere appreciation to the project supervisor, Assoc. Prof Chew Chee Meng who has been giving assistance, help and valuable recommendations to the author throughout the process in carrying out the work successfully.

Besides, the author would like to thank the following people for their assistance and encouragements during the process of implementing this project.

1) The members of Team ROPE especially Miss Wu Ning and Miss Meriam who have been working hard on the ROPE project.

2) Mr Li Renjun and Mr Shen Bingquan who have provided the author an insightful knowledge in terms of software and hardware.

3) Miss Hamidah who has been helping the author in getting the instruments for the experiment

4) The technicians, staff and graduates students in Control and Mechatronics Laboratories 1 and 2 for their untiring support, help and advice.

Table of Contents

Summary

This thesis presents a new foot system for biped walking on uneven terrain and its design flow. Stabilization of contact states between foot and ground and proper landing on unknown terrain are the criteria that ensure stable walking motion on uneven terrain. Generally, the conventional rigid and flat foot changes its contact states (separates from the ground) easily. In addition, the impulsive force exerted during landing on rough terrain must be suppressed. The author proposed a point-contact type foot with hydraulic fluid balance mechanism. The size of the proposed foot mechanism is 160 mm x 277 mm and its weight is 1.6 kg. The foot system consists of four contact points each of which equipped with a force sensing resistor (FSR) to detect the landing state. The foot generates a support polygon on uneven terrain by using three or four contact points. Stabilization of contact state, estimation of the zero moment point (ZMP) position, absorption of landing impact and faster response in achieving stable state are the main advantages of the proposed foot system. Landing pattern with dorsiflexion and plantarflexion are proposed to further increase the adaptability of the proposed foot on higher raised platform. Several experiments are conducted on the even ground surface, 10mm bumps, 15mm bumps and slope with gradient of 7.0 degrees, and the effectiveness of the foot mechanism is demonstrated through the experiments.

List of Tables

List of Figures

Abbreviations:

Centre of Gravity	COG
Centre of Mass	COM
Force Sensing Resistor	FSR
Sum of Squares for Error	SSE
Zero moment point	ZMP

Chapter 1: Introduction

1.1 Background

High adaptability on uneven terrain is the key feature for biped walking motion. This feature enables bipedal robots to integrate into human living environment easily. Thus, the bipedal robots that equipped with this ability are required to assist human beings in various fields. Various researches on biped walking motion on uneven terrain have been widely studied. However, stable biped walking motion on uneven terrain has not been realized yet.

Based on the definition of Sardain and Bessonnet [35], walking motion can be divided into two main phases, which are single support and double support phases. During the single support phase, the supporting foot takes off from the ground and the supporting ankle rotates about the supporting toe. During double support phase, the swinging leg lands on the ground. These two phases will be repeated in turn to generate a periodic motion. This kind of periodic motion enables the biped robot to walk forward as the center of mass of the robot is moved forward during single a walking cycle. However, improper landing and excessive impact force could occur during the initial contact state. In order to achieve stable walking on uneven terrain, the bipedal robot has to stabilize itself with respect to the contact states between foot and ground while landing on the unknown terrain. Bipedal robot would fall down easily if the centre of mass of the bipedal robot is located outside the support polygon. For bipedal robot, the support polygon refers to the convex hull generated by the supporting foot or feet on the ground. Landing state stability is highly relying on the foot placement onto the contact ground. Proper foot placement would prepare a large support polygon whereas improper foot placement would reduce the support polygon of the bipedal walking robot. Assessing foot placement and correcting the landing pattern is vital for fall prevention.

In order to generate stable bipedal walking motion on uneven terrain, some researchers have studied the motion pattern generation methods while other researchers have researched on real-time stability control methods [2, 11, 38, and 48]. During single support phase, most of the studied methods have been assuming that the contact state of the foot is supported by four contact points. However, this assumption is not applicable for a bipedal robot that is walking on uneven terrain.

As a bipedal robot moves its center of mass (COM) during single support phase, the contact state between the foot and the ground determines the walking stability for subsequent walking cycle. For bipedal robot that equipped with rigid and flat foot, it is challenging for the robot to maintain its foot in contact with the rough terrain because the foot changes its contact state easily and randomly. As shown in Figure 1, when the bipedal robot with rigid and flat foot is walking on an uneven terrain, a relatively small support polygon would be formed by its foot due to the absence of four-point contact state [15, 26]. The red triangle indicates the support polygon. On the uneven terrain, with the flat and rigid foot, there might be two to three contact points formed in between the foot and the contact ground. Hence, it is difficult to keep the zero moment point (ZMP) in the small support polygon even if the moment compensatory method is implemented [49]. ZMP can be defined as the point on the ground where the net moment of the gravity forces and the inertial forces has no horizontal component [27]. The moment compensatory method is applied to control the walking motion such that the ZMP is within the support polygon. For stable walking motion on uneven terrain, the control methods and foot systems design should be improved simultaneously.

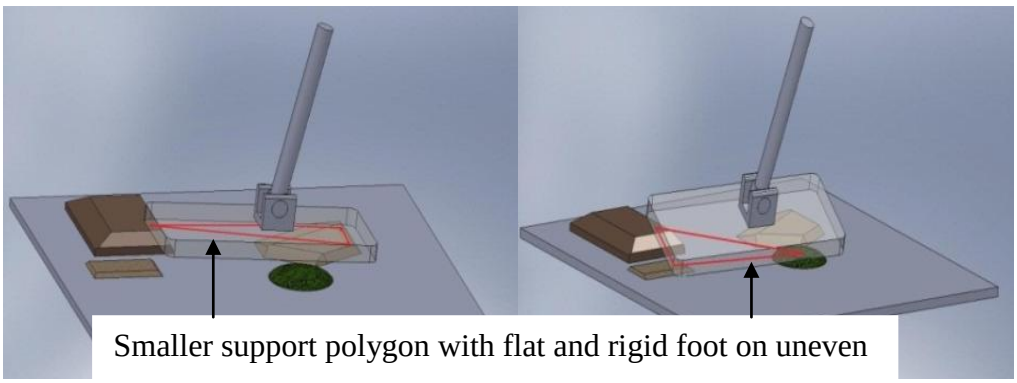

Figure 1.0: Rigid and Flat Foot in contact with uneven terrain

1.2 Problem Definition

According to Kim et al. [12], uneven terrain can be defined by a combination of global and local inclination. Global inclination refers to the terrain with a constant slope. On the other hand, the local inclination refers to the slope where the foot is landing or supporting. They proposed a control algorithm for the biped walking on uneven terrain. However, the contact state where the robotic foot lands is assumed to be perfectly flat. Most of the bipedal robot researchers also made the same assumption. However, this assumption could not reflect the real situation at the contact state. The contact state of the foot may be full of random irregularities as well. Hence, a new classification of the rough terrain has been proposed by Yamada et al. [30]. The new classification is shown in Figure 1.1. As shown in Figure 1.1, the combination of the global, local and micro fluctuations defined the uneven terrain. Global fluctuation refers to the fluctuation with constant inclination. Local fluctuation refers to the fluctuation that is flat with respect to the contact foot. Micro fluctuation refers to the fluctuation that is full of random irregularities. Hence, the proposed foot system is designed such that it could adapt to the unevenness defined by Yamada et al. [30].

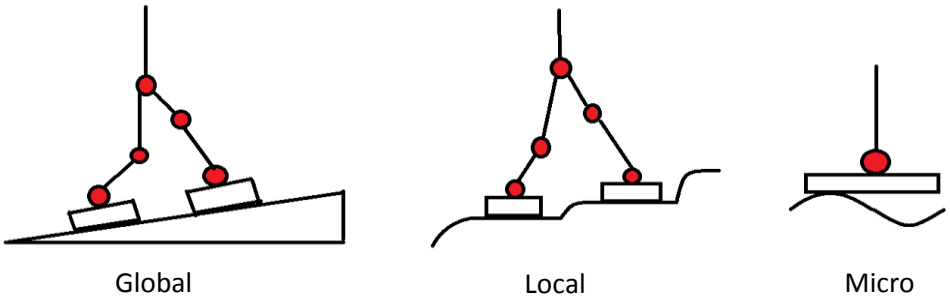

Figure 1.1: Classification of rough terrain (Kim et al. [12])

The consequences of improper landing have been discussed by Yamada et al. [30]. Figure 1.2 below summarizes the consequences if the landing state of the walking robot is unstable. Unstable contact state could be defined as the state where the number of contact points is less than 3[14, 41, and 50]. Landing on unstable contact state would result in improper landing which would trigger the destabilization of the contact state between the foot and the ground. Excessive impulsive force would be exerted on the landing foot is swing foot is landing on unstable contact point. Destabilization of the contact state and the excessive impulsive force would decrease the walking motion stability. If the contact state is unstable, the walking motion controllers may not able to be implemented at the correct timing. Hence, a new landing pattern together with a new robotic foot system is proposed.

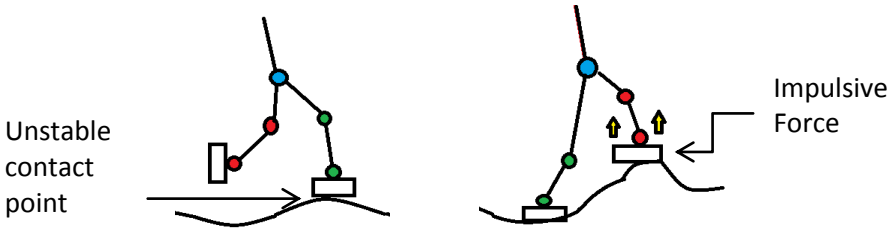

Figure 1.2: Problems in walking on rough terrain

1.3 Objective

Based on the reviews in previous section, in order to achieve stable walking motion on uneven terrain, there are two general approaches: control based algorithm and foot system design. The first approach makes use of various control theories or algorithms to achieve walking on uneven terrain. Normally, this approach is relatively more complicated as it needs high computational power and high precision sensor inputs. In the second approach, the focus is on the foot system design and the landing state. This approach is relatively less complicated but it is normally passive in nature which will function only when there is activation on the foot system. Hence, in order to minimize the research gap between the two approaches, the author has come out with a new foot system design together with new landing pattern control. This is a complementary step for walking on uneven terrain. The proposed foot system is a combination of **s**hock absorbing mechanism, landing surface detection mechanism and stabilization mechanism of supporting leg and landing leg. The proposed foot system is equipped with simple controller to activate the foot system mechanism. The working principle of the proposed foot system is based on the Pascal's Law. Pascal's law states that if pressure is exerted at any point within a confined incompressible fluid, the pressure will be transmitted equally in all directions throughout the fluid so that the pressure difference in the fluid remains the same as the initial value [24]. Ideally, the proposed foot system would balance by itself by transmitting the impact on the foot equally during landing state. In other words, the proposed foot system is a proactive device. Besides, the proposed foot system is working with a new landing pattern to increase it adaptability on uneven terrain. This design does not only simplify the controller for uneven terrain walking motion but also increase the stability of walking motion.

1.4 Thesis Outline

This dissertation discusses the design flow for a new proposed foot system which is used for biped uneven terrain walking motion. This thesis has the following structure:

Firstly, an extensive research covering the theories and principles required for the proposed foot system design are analyzed. Moreover, the reviews for foot system design in the current development for uneven terrain walking motion are studied in Chapter 2. All the current foot system designs and research provide a good inspiration and foundation for the author. Given the comprehensive overview of biped walking on uneven terrain, this thesis introduces the design flow that guides to the entire design process of the proposed foot system. Also, a landing pattern that mimicked human landing pattern is further discussed. Thirdly, it describes the hardware and software architecture of the proposed foot system. Next, the experimental results for the proposed foot are discussed. Some comparisons are made for the cases with and without the proposed foot system. Furthermore, the problems of the proposed foot system are identified in the same section.

Lastly, a summary for the whole thesis is made to conclude the feasibility and functionality of the proposed foot system. The potential of the proposed foot system for future development is listed. Also, the current development and future prospects of the research on foot system design are discussed.

Chapter 2: Literature Review

In this Chapter, the reviews for foot system design in the current development for uneven terrain walking motion are studied. This review provides the design ideas to the author.

Besides, the walking motion and landing pattern are analyzed in Chapter 2. This analysis would provide the design requirements for the proposed foot system. With these design requirements, the working principle of the proposed foot system would be discussed in Chapter 3.

2.1 Overview of Current Technology on Uneven Terrain Walking Motion

Although there have been a lot of research works done on the stability control of biped robot on uneven terrain [4, 6, 7, 15, 18, 26, 36, 43], most of them have assumed that large and stable support polygon could be maintained by the biped robot on uneven terrain. However, outdoor environment is full of random and unknown irregularities that could hinder the biped robots with rigid and flat feet from maintaining large support polygon. This implies that the robots could lose theirs balance easily even if stability controller is implemented. Ideally, the necessary condition for stable walking motion on uneven terrain is where the biped robots should be able to maintain four-point-contact with ZMP maintained at the centre of the foot during the whole walking cycle. The paper which was presented by Hashimoto [14] described a new foot system, WS-1 (Waseda Shoes - No.1) that is able to maintain four points contact at the contact state. This foot system makes use of cam-type locking mechanisms. It is controlled actively according to the contact points. However, due to improper sensors mounting landing state detection is not very accurate. Hence, Hashimoto et al. [16, 17] has developed a new biped foot system, WS-1R (Waseda Shoes - No. 1 Refined) which can maintain large support polygon on uneven terrain. This biped foot system is equipped with four contact points at each corner of the foot. When all the contact points

follow the unevenness of the contact ground, all the contacts point would be locked. Nevertheless, this design could not deal with concave surface where the large support polygon could not be maintained. This is because the foot designed by Hashimoto [16, 17] did not allow any extension of the contact point. Hence, the locking mechanism could not be triggered to maintain large support polygon. This scenario is shown in Figure 2.1 below.

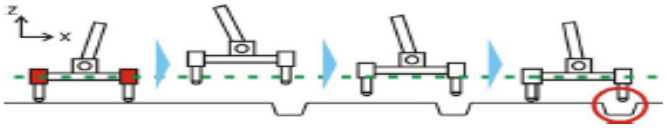

Figure 2.1: Deficiency of the foot design proposed by Hashimoto et al. [16, 17]

Also, this design is heavier (1.9 kg) than conventional rigid and flat feet. Heavy ankle would reduce the swing speed of the swinging leg and reduce the stability of the supporting leg. Then, Hashimoto et al. has improved the four-point contact type foot by using actuators [13]. This design could adapt to irregularity on the ground which include concave surface. Although it can adapt to rough terrain semi-actively, the actuators increase the weight of robot and decrease the energy efficiency. Furthermore, this design is not rigid and could not suppress the impact force during foot landing [13].

Rubber pad mechanism has been installed at the feet of the testing bipedal robot to stabilize the contact states [18, 21]. Nonetheless, the soft material could not effectively adapt to uneven terrain because the shape of the soft material cannot be maintained during single support period. Ideally, the foot system should able to adapt to the unevenness and retain the shape during single support period. Yamaguchi has proposed a foot mechanism (WAF-2) which utilizes a shock absorbing material that could detect the unevenness of the landing surface [10]. The foot system proposed by Yamaguchi had improved the walking stability of biped loco motor WL-RIII through various walking experiments [10]. However, this design could not be used to adapt to the rough terrain with global inclination. Subsequently, Yamaguchi et al. has

improved the foot system by installing a buffer and a sensor on the new foot system [11]. The buffer system is used to absorb the landing impact force whereas the sensor is used to detect a step on uneven terrain. Notwithstanding, the foot system has a complicated structure which makes it difficult to be applied to rough terrain with micro fluctuations.

Sano and Yamada have proposed a new point-contact type foot with springs (PCFS) [41]. This proposed foot could adapt to rough terrain by minimising the impact force and disturbance. In addition, the stability index which refers to zero moment point (ZMP) and the posture of robot can be estimated by measuring the displacement of each spring installed on the foot. The control algorithm proposed by Sano and Yamada [41] could only work on low spring constant mechanism. The foot systems of H6 and H7 which were proposed by Nishiwaki et al. [22, 24] are equipped with toe joints which enable the robot to walk with higher speed and larger steps length. Nevertheless, this design is not suitable for uneven terrain with micro and local fluctuation. HRP-2 [20, 39] and ASIMO [19, 25] have been equipped with impact absorption mechanisms as well. Notwithstanding, these foot mechanisms are having difficulties in maintaining four points contact state on uneven terrain.

2.2 Walking Motion

Proper landing requires appropriate landing pattern. In this section, the landing patterns that fit to the proposed foot design would be discussed.

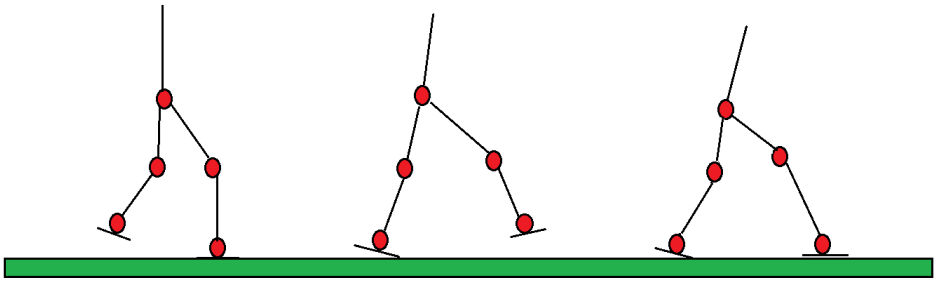

Figure 2.2: Fully actuated phase, the under actuated phase, and the double-support phase respectively [35].

Based on the definition of Sardain and Bessonnet [35], a fully actuated phase, an under actuated phase, and a double-support phase in succession contribute to a complete bipedal robot walking cycle. All the mentioned phases are illustrated in Figure 2.1 above. During fully actuated phase, the supporting foot is flat on the ground. The supporting foot takes off from the ground and the supporting ankle rotates about the supporting toe during under actuated phase. During double support phase, the swinging leg lands on the ground. In order to simplify the position control on the leg movement, the swing foot is assumed to be parallel to the ground at impact during the double-support phase. It is also assumed that the foot has an arc shape structure which has contact points with the ground at the heel and toe. Nevertheless, these two assumptions could not be applied in real case due to the fact that a rigid and flat foot is used especially on uneven terrain. Figure 2.2 indicates the shape of the foot that equipped with contacts points. Via Figure 2.2, for the arc-shaped foot, the ground contact forces can be resolved into a force vector and a torque. Hence, when the swinging foot is landing on the ground, the impulsive forces

would be exerted at the toe and the heel simultaneously. This impact could result in discontinuation in the changes of velocities. Nevertheless, the position states are assumed to remain continuous [45].

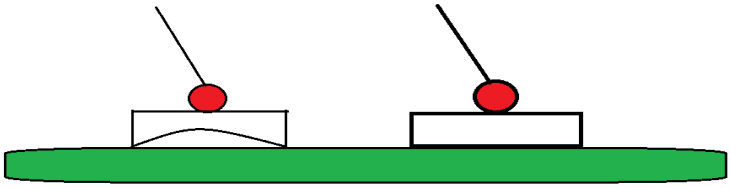

Figure 2.3: Examples of foot shapes with point contacts: (a) arc-shaped foot and (b) flat foot

For the case of the flat foot, the ground contact forces can be resolved into a force vector and a torque if the contact ground is flat. If the contact ground is uneven, the heel and toe of the swing foot might not land on the ground simultaneously. The landing impact would result in rebound and slipping of the swing foot. Subsequently, the walking motion controller would become more complicated. In order to solve this problem and uphold the assumptions stated above, the author has proposed the foot system with four contact points. In the following section, fully actuated phase, under actuated phase, and double-support phase would be discussed in further from the view of ZMP stability index. The stability index provides the design requirements of the proposed foot system.

2.3 ZMP Stability Index

The ZMP has been widely used as a necessary stability indicator for bipedal robot [27]. During bipedal walking motion, the ZMP being within the support polygon is a sufficient and necessary condition to prevent the rotation of supporting ankle. For a bipedal robot that has a walking gait consists of the fully actuated phase and then followed by an instantaneous double-support phase. The ZMP has to be kept within the support polygon during the fully

actuated phase in order to ensure that the supporting foot is remained flat on the contact surface. This necessary condition is used to ensure that the supporting foot does not rotate.

Definition:

"The ZMP criterion states that when the ZMP is contained within the interior of the support polygon, the robot is stable, i.e., will not topple [1]."

Hence, this ZMP criterion would be used to estimate the walking motion stability.

2.3.1 Direct Control of the Zero Moment Point (ZMP)

The concept of controlling the ZMP point has been used in the majority of bipedal robot control algorithms. Generally, these control strategies can be divided into error tracking controller and error minimizing controller. The error tracking controller ensures the correct tracking of the reference ZMP whereas the error minimizing controller modifies the reference motion to ensure the ZMP point remains within the foot support polygon. Nonetheless, with flat and rigid foot on uneven terrain, it is difficult to generate a walking gait that could ensure the ZMP point is within the foot support polygon. As long as the ZMP point remains inside the foot support polygon, the supporting foot would not rotate. In order to ensure that the supporting foot is remained flat on the ground, the ZMP must never reach the limits of the foot support polygon. Direct control of the ZMP position is used to prevent the mentioned scenario. In the following sections, the position of ZMP during fully actuated phase, under actuated phase, and double-support phase would be discussed to ensure the ZMP criterion is satisfied throughout a walking cycle.

2.3.2 Ideal ZMP Position during Under Actuated Phase

During the under-actuated phase, the supporting ankle of the robot takes off from the ground. Then, the robot progresses via foot rocker over the supporting toe. At this moment, the position of zero moment point (ZMP) is strictly in front of the supporting foot. The supporting toe acts as a pivot for the progression. There must be no sliding or slipping at the toe joint. In the proposed foot system design, the conditions for ZMP position and non-slippage during this phase are the constraints that must be imposed. A new foot system with flexible four contact points and plantarflexion landing pattern is required to satisfy the ZMP criterion.

2.3.3 Ideal ZMP Position during Fully Actuated Phase

The supporting foot is assumed to maintain flat on the contact surface without slippage during the fully actuated phase. The ankle of the supporting leg acts as an actuated pivot for foot rocker progression. In order to satisfy the condition that the supporting foot is flat on the contact surface, the ZMP point has to be kept strictly within the support region of the supporting foot. The position constraints for ZMP must be imposed in the foot system design. However, for rigid and flat foot on uneven terrain, it is difficult to uphold these conditions.

2.3.4 Ideal ZMP Position during Double-Support Phase

During double support phase, the bipedal robot is supported by swing leg and supporting leg during this short period. The impact exerted during the instantaneous double-support phase would introduce disturbance to the walking motion. Although the landing impact could be suppressed via algorithm and controller design, this would make the dynamic of the walking motion more complicated. Hence, the proposed foot system should have the ability to reduce the landing impact during walking motion.

Chapter 3: Design Flow and Working Principles

In this section, the design flow for the proposed foot system is discussed in detail. In order to achieve stable walking motion on uneven terrain, stable landing state should be provided so that the subsequent walking motion controllers could be implemented at the correct timing. The ZMP of the robot should be maintained within the support polygon of the stance foot. A bipedal robot could easily maintain its ZMP within support polygon when it is walking on flat ground. However, it is relatively difficult for the robot to maintain the ZMP within the support polygon when the contact ground is uneven.

A new foot system with four contact points is proposed to solve the problem. The ZMP can be maintained at the center of the foot which could ensure that the ZMP is always lying within the support polygon. By combining the conditions and constraints mentioned in Chapter 2, the design objectives of the proposed foot system design are listed as follows:

1) The position of ZMP must be maintained in front of the standing foot during under actuated phase. Also, free of foot rotation and nonslip are the constraints that must be imposed.

2) During fully actuated phase, the supporting foot has to be flat on the ground and the ZMP point needs to be maintained strictly within the support polygon of the foot.

3) During double support phase, the impact landing should be absorbed to prevent to variation of ZMP position from the support polygon of the foot.

Given the design objective, the design considerations for the proposed foot system could be summarized as follows:

- Absorption of landing impact
- Rapidly reach stable contact state
- Rapidly become rigid after stable contact state is achieved
- Estimation of ZMP position
- Simple and light weight (few sensors, no active actuation)

The design objectives and considerations are used to generate the foot system design in the following section.

3.1 Design Ideation, Structure and Advantages

The proposed foot system should be able to maintain the four contact points all the time when it is in contact with the uneven terrain. Subsequently, the ZMP could be maintained inside the foot support polygon to ensure that the supporting foot does not rotate about its edges.

Based on the design objective sand considerations in the previous section, a new foot design which is based on Pascal’s law is proposed. Pascal's law states that if pressure is exerted at any point within a confined incompressible fluid, the pressure will be transmitted equally in all directions throughout the fluid so that the pressure difference in the fluid remains the same as the initial value [24].The Pascal's law is referred to the principle of transmission of fluid-pressure.

The proposed foot system is shown in Figure 3.0. The proposed foot system consists of foot sole sensor and sensor fusion architecture. The new proposed foot system has high adaptability on uneven terrain being able to maintain stable contact with the ground at four points around four corners, estimate the

position of ZMP by using force sensing resistors, high absorbability of landing impact and disturbance rejection.

The proposed foot is attached with four hydraulic cylinders with a maximum stroke of 25mm which are interconnected by polyurethane tubes such that fluid exchange can be enabled among them. It is difficult for biped walking robots to walk stably on uneven terrain with 20 mm fluctuation even when a real-time stability control method is employed. Hence, the vertical movable range of a new foot system is set at 25 mm. The excess 5mm is provided for further allowance. Ideally, the proposed foot system is "locked" when all the four contact points are in contact with uneven terrain and the ZMP is near to the centre of the foot. When the proposed foot system is "locked", the fluid exchange is stopped and the foot is maintained at that particular orientation. However, four points contact is difficult to achieve in practice. A more practical locking condition would be discussed later. Besides, if flat foot landing pattern is applied together with the proposed foot system, the maximum adaptability of the proposed foot system on a raised platform is only 25mm. This is due to the limitation of the stroke of the hydraulic cylinder. In order to increase the adaptability of the proposed foot system, dorsiflexion and plantarflexion landing pattern is proposed. The details discussion for the landing pattern would be discussed in the latter chapter.

Three solenoid valves are used to 'lock' or 'unlock' the fluid exchange among the cylinders. Figure 3.1 indicates the hydraulic circuit of the proposed foot. Fluid exchange among the cylinders should be stopped instantaneously when the locking condition is satisfied. Four force sensing resistors (FSR) are connected to the four contact points to detect the landing state. By using the principle of Pascal's Law, when one or more of the contact points is in contact with the terrain, fluid exchange would be triggered until all the four contact points exert the same pressure to the contact terrain. The hydraulic fluid exchange among the four hydraulic cylinders is to ensure that the stabilization

of the proposed foot system is in two dimensions which refereed to pitch and roll axes of the testing robot. At this moment, the locking mechanism is enabled to stop the fluid exchange among the cylinders such that the four contact points are maintained at the position such that the ZMP is near to the centre of the foot. The working flow chart of the proposed foot system is summarized in Figure 3.2. Each of the steps would be discussed in detail in the following section.

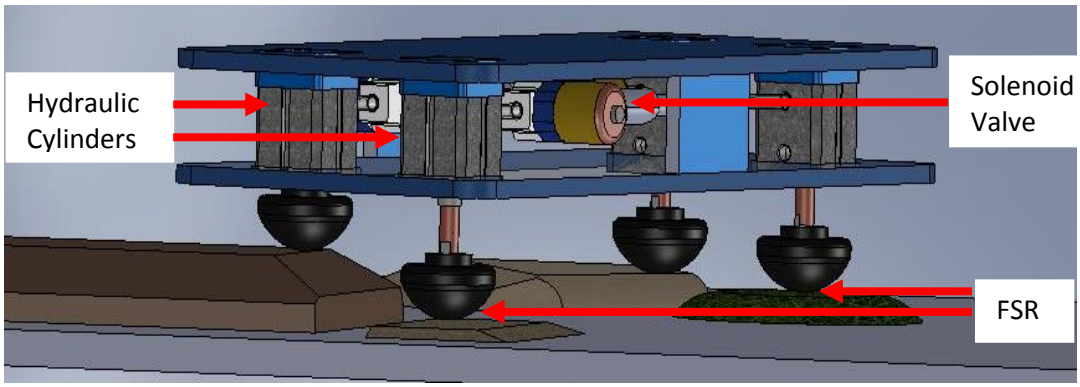

Figure 3.0: Proposed foot system in CAD

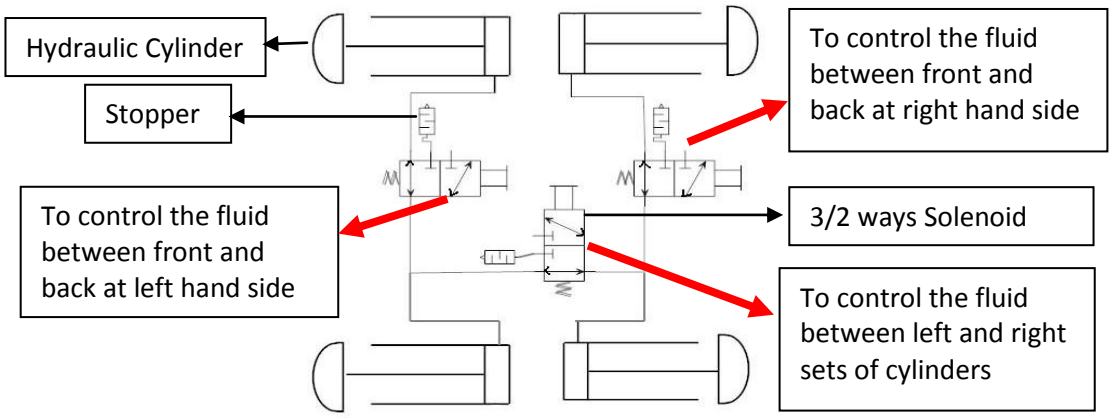

Figure 3.1: The hydraulic circuit of the proposed foot system

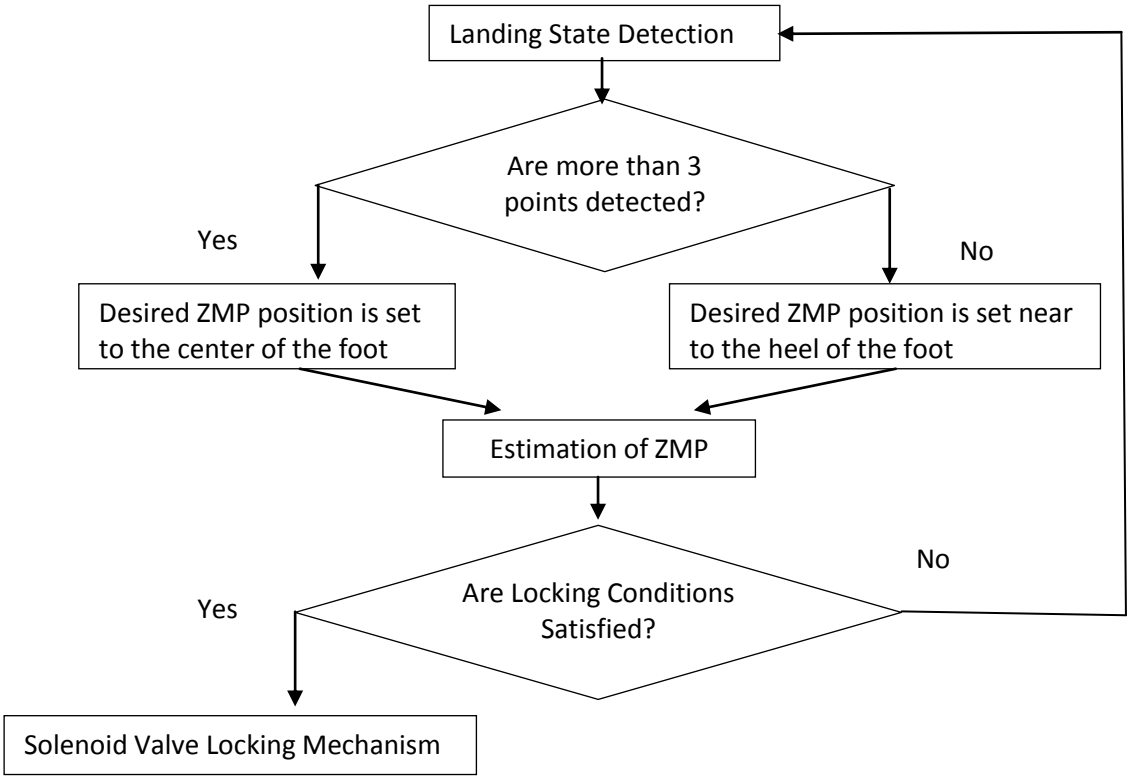

Figure 3.2: Working flow chart of the proposed foot system

3.2 Working Principle of the Proposed Foot System

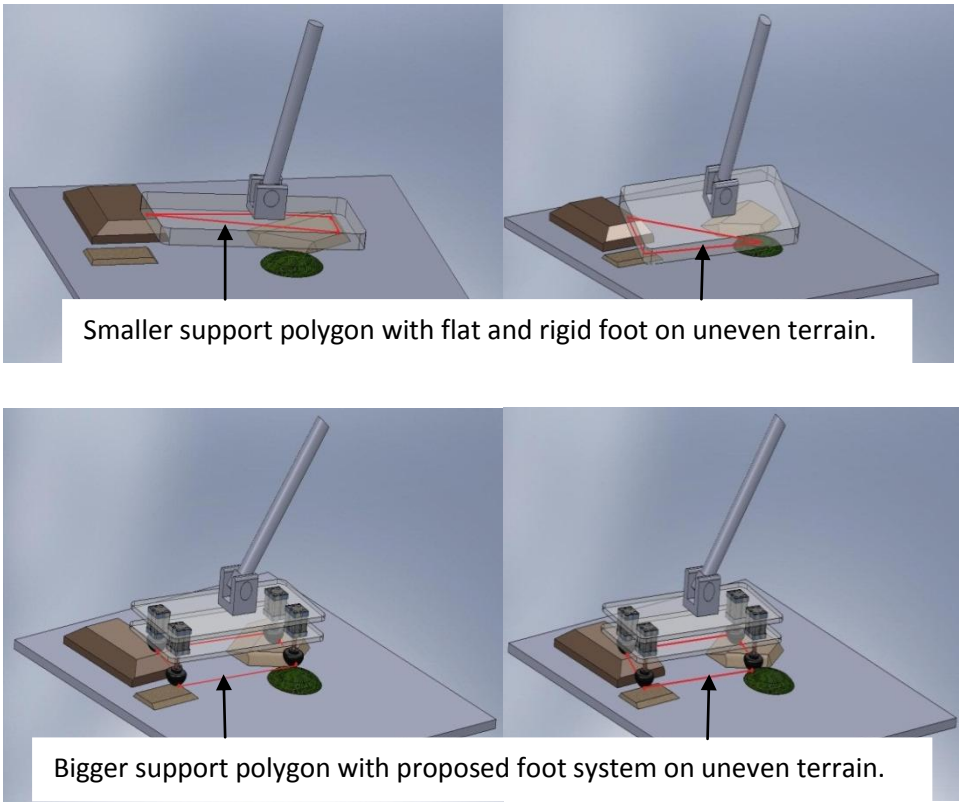

Figure 3.3: Working principle of the proposed foot

There are two main functions of the proposed foot, viz.: landing state stabilization and ZMP estimation. This section would discuss each of this function in detail.

3.2.1 Landing State Stabilization

This section describes the stabilization of the landing state by the proposed foot system. The stabilization of the proposed foot is done via the landing impact absorption and the control of the ZMP position. Landing impact is absorbed via the fluid exchange within the hydraulic cylinders. The landing impact is converted into the energy that is used to move the hydraulic cylinders. Based on Pascal's law, the fluid exchange enables the regulation of the ZMP position. The fluid exchange is stopped if the ZMP is positioned at

the center of the support foot. However, in the worst case, if the ZMP value is maintained at the corner for long time, the robot has to take another step to regain stability,

3.2.2 Stability Index Estimation

This section describes the estimation of the stability index, ZMP, by using the proposed foot system. The ZMP is the necessary stability index to indicate the walking motion stability. For the case of rigid and flat foot on uneven terrain, the ZMP is difficult to be estimated because the contact state changes easily. Since the proposed foot system has only four contact points, the ZMP can be estimated easily by measuring the reaction force that exerted on each contact point. From the magnitude of reaction forces and the positions of the contact points, the position of ZMP p = (px, py) can be determined via the equation 3.1 below:

$$p = \frac{\sum_{i=1}^{4} f_i p_i}{\sum_{i=1}^{4} f_i} \quad \text{---------- (3.1)}$$

Where fi (i = 1 ...4) is the normal reaction force (with respect to the contact surface) that exerted on each contact point and pi = (pxi, pyi) is the two dimensional position vector of each contact point. Figure 3.4 indicates the layout of the FSRs on foot plate. The estimation of ZMP is according to the dimensions in Figure 3.4.

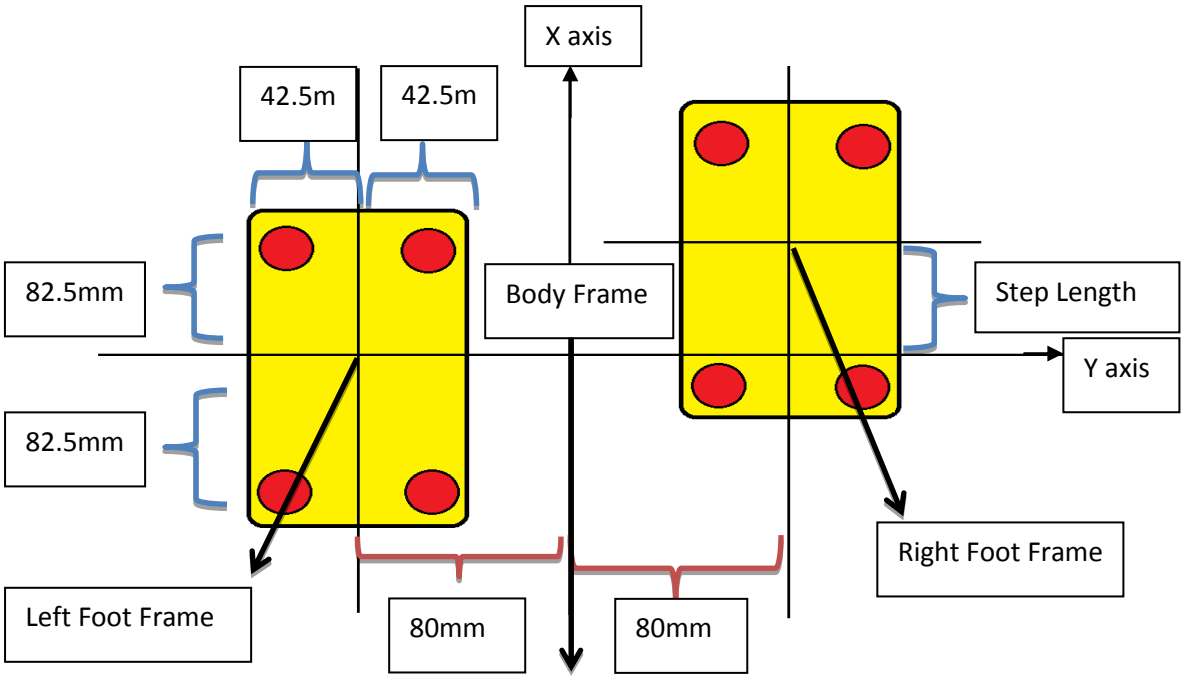

Figure 3.4: The layout of force sensing resistors on foot plate

3.3 Locking Mechanism

Locking mechanism is the most important element for the functionality of the proposed foot system. This mechanism should able to sustain landing impact and then maintain the locking function during walking motion. The foot system would become heavy if the locking mechanism is complicated. Heavy foot would reduce the swinging leg velocity and hence reduce the gait velocity and stability. Hence, a simple but robust locking mechanism is required. The locking mechanism must be locked instantaneously in an arbitrary position so that the foot could continuously follow the fluctuation of the contacting surface. Also, since the design foot is to ensure the ZMP stays closes to the middle of the ankle, the locking mechanism must be triggered right before the COM moves from supporting leg to swinging leg, regardless of contact state conditions. The locking mechanism is based on the bang–bang controller.

3.3.1 Locking and Unlocking

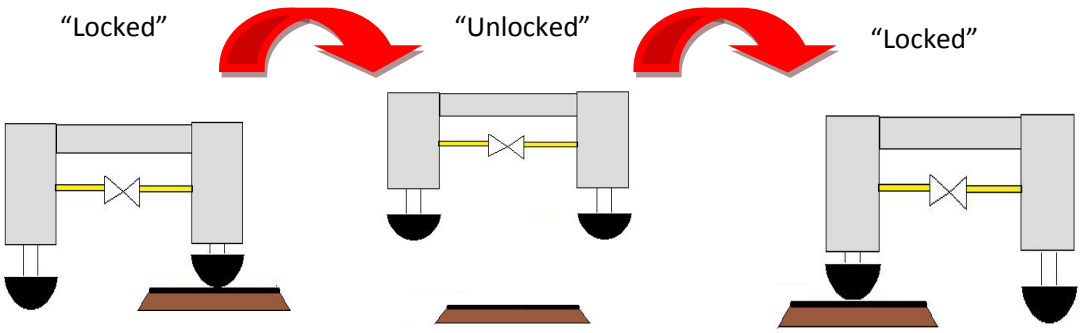

Figure 3.5: Locking and unlocking conditions (side view)

Figure 3.5 above summarizes the locking and unlocking mechanism when a bipedal robot is walking on a raised platform. Ideally, when all the four contact points register approximately the same value (i.e. the ZMP is at the centre of the foot), the locking mechanism is applied. On the other hand, when all the four contact points register null values, the unlocking mechanism is applied. Four contact points are not easy to be achieved when the robot is walking on uneven terrain. Hence, a relatively less strict locking condition would be discussed in the following section.

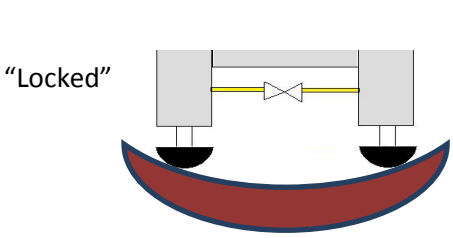

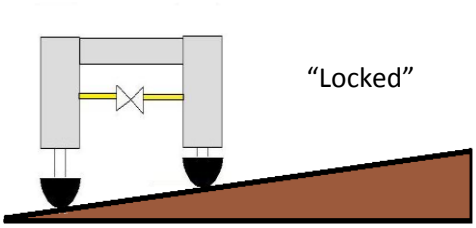

Figure 3.6 **Figure 3.7**

Figure 3.6 & 3.7: Adaptability on concave surface (3.6) & global inclination (3.7) respectively (side view)

By using the same locking mechanism, the proposed foot system can be used to adapt concave surface. This is shown in Figure 3.6 above. Besides walking on micro uneven terrain, the proposed foot system can be used to adapt to global slanted terrain. This is illustrated in Figure 3.7 above. Given the length

of the foot and the maximum stroke of the hydraulic cylinders, the maximum global angle that can be adapted by the proposed foot system is eight degree. The detailed calculation is as equation 3.2 below.

$$\theta = \tan^{-1}\left(\frac{stroke\ of\ the\ cylinder}{length\ of\ the\ foot}\right) \text{---------- (3.2)}$$

3.3.2 Locking Conditions Selection

In this section, a relatively tolerant locking condition would be discussed as a complementary constraint for the four points contact condition. The ideal condition for locking mechanism is where the four contact points on the proposed foot are detected and the ZMP is located near to the center of the foot. This necessary condition is required to ensure the landing state stabilization is in 2 dimensions which referred to pitch and roll axes of the testing robot. However, the four points contact might not easy to be achieved in practice. Hence, a compromised locking condition would be used if four contact points are not detected during initial landing state.

During initial landing state, if four points contact is not achievable, the locking mechanism would be based on three points contact. Given this initial condition(three points contact during initial landing state), the fluid exchange among the cylinders might not be fast enough to achieve stable four points contact where the ZMP is located near to the center of the foot. A foot mechanism that could maintain three-point contact has been designed by Shoji et al. for bipedal robot to achieve self-supporting on rough terrain [4]. This result has proven the tripod stability for bipedal robot. Although three-point contact foot has high adaptability on rough terrain, its support polygon is smaller than the flat and rigid foot on a flat surface. This implies that its stability margin is narrower than the case with four-point contact foot. However, the four-point contact state is not easy to be achieved in practice due

to the random and uneven fluctuations on the contact surface. Hence, the trade-off between the two has to be balanced. Generally, for walking on flat terrain, the four points contact state condition is preferred. For walking on rough terrain, the three points contact state condition is preferred.

If 3 or less contact points are detected during initial landing state, the ideal locking condition is where the ZMP is near to the rear foot. The ideal locking condition is defined as a region (circle) which is illustrated in Figure 3.8. This region is located along the x axis of the proposed foot system and it is placed at 5cm below the y axis of the proposed foot system. This region could be termed as stable region which is selected based on experimental result analysis where the robot could achieve stable landing state.

Bang–bang controller is used to control the on-off state of the solenoid valves because this controller could provide a quick and instantaneous output response. In terms of Bang-bang controller, the locking condition could be expressed as equation 3.2 below:

$u = +V$ (solenoid valves are 'locked') if $0 \leq r \leq R1$

$= -V$ (solenoid valves are 'unlocked') if $r \geq R1$ ---------- (3.2)

Where u is the control input, V is the control signal, r is the position of real-time ZMP from the origin of the stable region and R1 is the radius of the stable region. R1 is set to be 2cm based on experimental observations where the bipedal robot could maintain walking stability during walking motion.

In 'unlocking' state, fluid exchange is allowed whereas in the 'locking' state, fluid exchange is stopped.

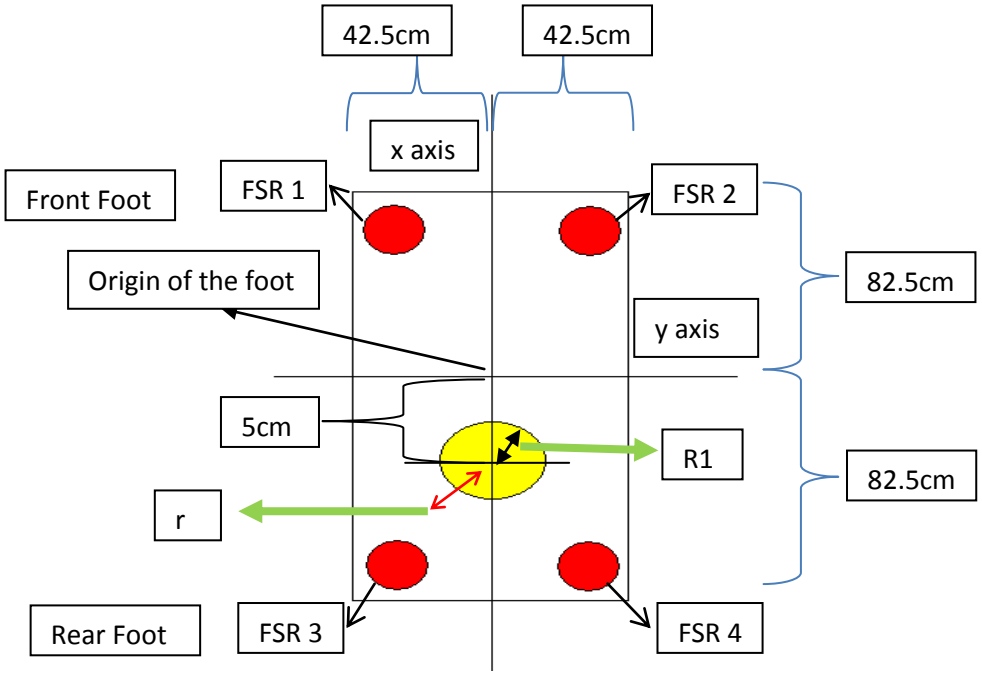

Figure 3.8: Desired ZMP position if 3 or less contact points are detected during initial contact state

If four contacts points are detected during initial landing state, the ideal locking condition is where the ZMP is near to the centre of the foot. The ideal locking condition is defined as a stable region (circle) which is illustrated in Figure 3.9. The origin of this region is coincident with the origin of the foot axis. This position is selected such that the walking robot could maximize the landing state stability.

In terms of Bang-bang controller, the locking condition could be expressed as equation 3.3 below:

$u = +V$ (solenoid valves are 'locked') if $0 \leq r \leq R1$

$= -V$ (solenoid valves are 'unlocked') if $r \geq R1$ ---------- (3.3)

Where u is the control input, V is the control signal, r is the position of real-time ZMP from the origin of the stable region and R1 is the radius of the

stable region. R1 is set to be 2cm based on experimental observations where the bipedal robot could maintain walking stability during walking motion.

For both locking conditions, as a safety measure, if the locking condition is not satisfied during mid-stance phase, the locking mechanisms would be triggered automatically.

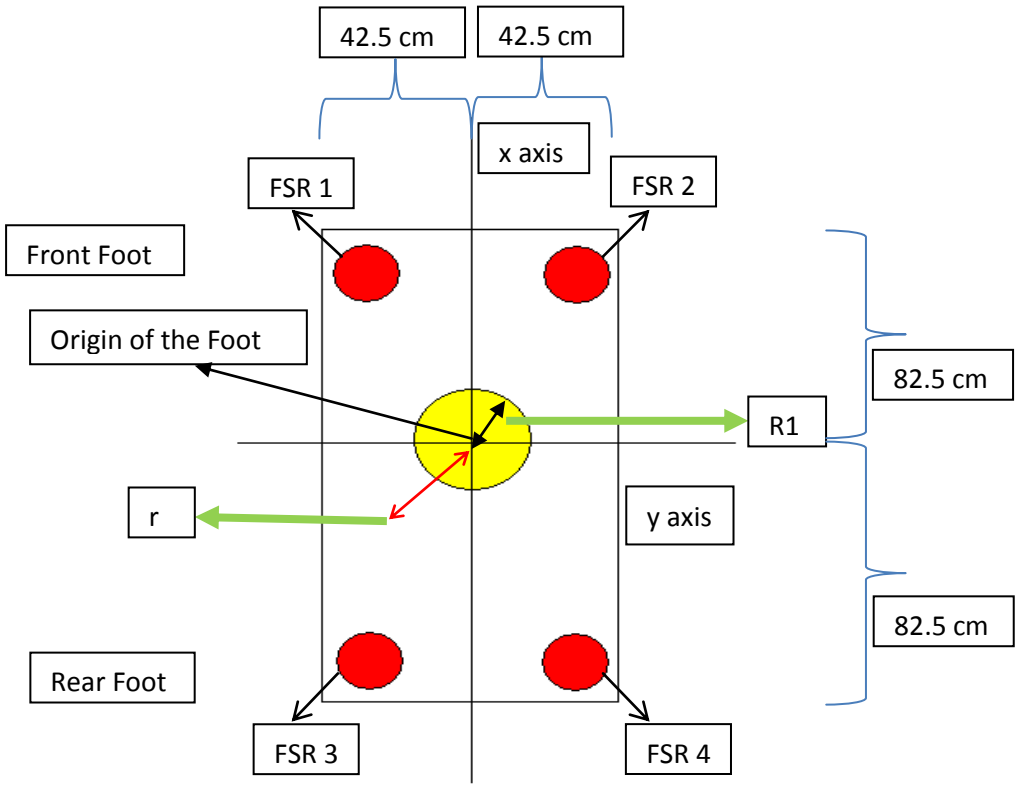

Figure 3.9: Desired ZMP position if four contact points are detected during initial contact state

Chapter 4: Landing Pattern

Although the maximum stroke of the hydraulic cylinders used is 25mm, the seal ring inside the hydraulic cylinders would slow down the rate of extension and retraction of the stroke. Since the friction is proportional to the extension or retraction rate of the stroke, for movement more than 10mm (based on experimental observation), the foot system would have difficulties to achieve equalled pressure on four contact points. This implies that if flat foot landing pattern is utilised, the maximum adaptability of the proposed foot system on a raised platform is 10mm.

Figure 4.1: Adaptability on a raised platform for the foot system with dorsiflexion and plantarflexion landing pattern (b) is higher than the foot system with flat foot landing pattern (a).

In order to further increase the adaptability of the proposed foot system, the proposed foot system has to be working together with predefined walking pattern. As shown in Figure 4.1, dorsiflexion enables the bipedal robot to land on a higher raised platform as compared with the case of flat landing pattern. Both cases are using the same ankle lift magnitude.

In this Chapter, two types of landing patterns will be discussed. They are flat foot and dorsiflexion- plantarflexion landing patterns. For the walking tests discussed in Chapter 6, flat foot landing is used when the robot is walking on even terrain and global inclination whereas dorsiflexion- plantarflexion landing pattern is used when the robot is walking on raised platform.

4.1 Flat Foot Landing

The following landing pattern is proposed to ensure flat foot landing that satisfied the stability conditions mentioned in the previous section. Flat foot landing refers to the type of landing that the foot is parallel to the ground during single support period (Figure 4.2). Ideally, the toe and heel have to be landed on the contact surface at the same time. This kind of landing pattern could provide maximum ground support during each step which is vital for a walking robot on even terrain. It could be used for bipedal walking motion at a slow or moderate velocity. This is because balance enhancing could be achieved via maximum support polygon size at every instant. The transition between single support phase and double support phase is performed with simultaneous flat contact of both feet.

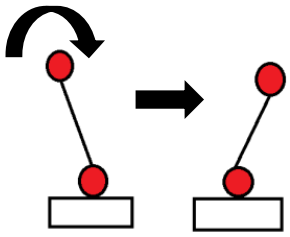

Figure 4.2: Landing foot is maintained flat in succession during single support period

4.2 Dorsiflexion and Plantarflexion Landing Pattern

Given the hardware constraints of the testing robot, the robot could only execute ankle lift of 20mm vertically. Therefore, the robot may adapt to a raise ground up to a maximum height of 10mm without losing any stability. In order to increase the adaptability of the walking robot on the terrain, the author has proposed a landing pattern which consists of dorsiflexion and plantarflexion. Figure 4.2 shows the way that plantarflexion is used to maximize adaptability on a raised platform. This landing pattern is inspired by human landing behaviour. Slight modification is done as the testing robot is not equipped

with toe joints. There are three main components in this kind of landing viz: progression, foot rocker and shock absorption [8]. The details of each component are further discussed as follows.

Progression

During the period when the fore foot of the swing leg has just taken off from the ground, the progression of the robot is initiated and the centre of mass (COM) of the bipedal robot progresses forward. Progression could be defined as the advancement of the COM of the bipedal robot during walking motion.

Foot Rocker

Once walking gait has been initiated, the advancement of the COM over the supporting foot depends on the foot rocker at the supporting leg. Foot rocker combine the effort of stabilization and progression to enable the advancement of the COM. The heel, ankle and forefoot rockers are implemented in succession to ensure continuous and stable COM advancement.

Shock absorption

At the end of the single support period, the ZMP of the robot might be beyond the stability margin due to landing impact. The resulting loss of stability may cause the bipedal robot to fall down. The landing impact could be minimized via ankle plantarflexion and ankle roll eversion which is followed by heel contact [9].

4.2.1 Ankle Trajectory for Dorsiflexion and Plantarflexion Landing Pattern

In this section, the ankle trajectory for dorsiflexion- planter flexion landing pattern at different walking phase is further analysed. This analysis is vital to derive the ankle trajectory into mathematical equations. According to Perry [8], this landing pattern consists of several phases which include initial contact phase, loading response phase, mid stance phase, terminal stance phase, pre-

swing phase, initial swing phase, mid swing phase and terminal swing phase. The details of each phase would be discussed in detailed in this section as well. Figure 4.3 below summarizes the leg trajectory during a walking cycle.

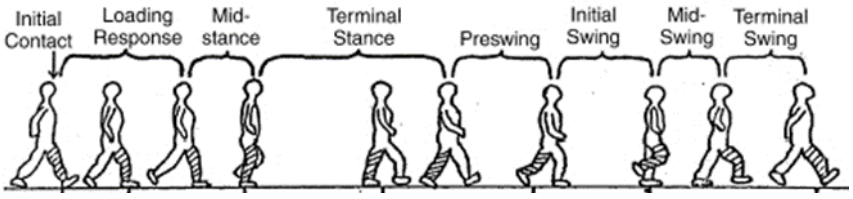

Figure 4.3: Leg Trajectory during a walking cycle [37]

Initial Contact (0 % to 2 % of the Walking Cycle)

In this phase, the heel rocker and impact deceleration are initiated as landing impact would be exerted on the landing foot. Generally, foot should have the ability to absorb the landing impact. As shown in Figure 4.4, dorsiflexion of 15 degree with respect to the landing terrain is implemented to concentrate the landing impact at the heel. An immediate but brief peak ZMP movement can be identified on the landing foot. This peak is termed as heel strike transient (HST) according to the definition by Perry [8].

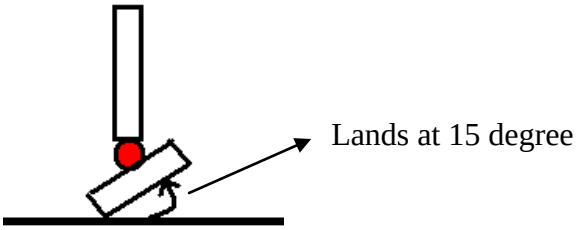

Figure 4.4: Dorsiflexion

Loading Response (2% to 12% of the Walking Cycle)

This phase is used to generate heel rocker initiation of progression and realignment of the ankle axis. Ankle plantarflexion and ankle roll eversion is implemented in this phase. Plantarflexion of 5 degree with respect to the contact surface is generated during 6% of walking cycle. Heel rocker is initiated to implement plantarflexion which would prevent the shank from advance too fast. Next, shock absorption mechanism is triggered. Plantarflexion transits to dorsiflexion as the ZMP is shifted towards the front foot. The end of the loading response is indicated by front foot contact.

Mid Stance (12% to 30% of the Walking Cycle)

The main functions of this phase are ankle rocker progression, ankle shock absorption and tripod for the support of stability. First arc of single stance dorsiflexion is implemented during this phase. At the end of mid stance phase, swing leg progression is slowed down to nearly half of its initial velocity during the start of the mid stance phase.

Terminal Stance (31% to 50 % of the Walking Cycle)

This phase is used to generate forefoot rocker for progression. Heel rising, ankle dorsiflexion continuation and reduction of ankle eversion are implemented in sequence. The body weight is supported only by forefoot. Progression is continued through forefoot rocker which ensures the body vector to advance further.

In order to reach a final position of 10 degree plantarflexion with respect to the ground, the ankle increases 5 degree in dorsiflexion. The heel is elevated via forefoot rocker which enables the height of COM to be maintained. As compared to the velocity during loading response phase, the velocity of shank (tibia) advancement is reduced to almost half. The plantarflexion is used to ensure both the foot and the shank (tibia) to roll forward on the forefoot rocker

which in turn provides ankle stabilization. Ankle stabilization could reduce the amount of fall by the centre of mass of the body and then makes its progression further. Roll off is triggered through the forefoot rocker. The COM advances across the forefoot as the heel is elevated with continuous forward progression. Meanwhile, dorsiflexion is increased to facilitate progression. ZMP is moved to the centre of the foot. The terminal stance phase is ended when ground contact is detected at the other foot.

Pre-Swing (50% to 62% of the Walking Cycle)

This phase is used to generate propulsion and initiation of knee flexion for swing. Second arc of ankle plantarflexion is implemented in this phase. Continuous forefoot contact enhances the balance of COM. Active ankle and foot stabilization is no longer required. Plantarflexion is continued at the ankle joint. The trailing foot is maintained at the terminal contact of the toes with the ground. This posture provides toe rocker for the leg advancement. Ankle plantarflexion to 15 degree (a 25 degree arc from the starting 10 degree dorsiflexion) is implemented via recoil thrust. As the ZMP is located at the forefoot, the foot is free to plantarflexion. Hip joint is moved toward neutral position to prepare for leg swinging.

Initial Swing (62% to 75% of the Walking Cycle)

This phase is used to generate floor clearance for leg progression. Second arc of dorsiflexion is implemented during this phase. The ankle introduces 15 degree plantarflexion with respect to ground during “toe off”. The shank (tibia) is left behind the body. Then, dorsiflexion is implemented for subsequent floor clearance when the shank (tibia) becomes more vertical. By the time the swinging foot is opposite the supporting leg, the swinging foot is maintained at neutral position which is equivalent to 5 degree of plantarflexion.

Mid Swing (75% to 87% of the Walking Cycle)

This phase is used to further generate floor clearance. Ankle dorsiflexion is continued from the previous phase. In order to achieve neutral ankle position, ankle dorsiflexion to neutral or a couple of degrees above the horizontal axis is accomplished.

Terminal Swing (87% to 100% of the Walking Cycle)

This phase is used to prepare for initial contact phase of the next walking cycle. The ankle is supported at neutral. With 3 to 5 degree decrease in plantarflexion, optimum heel contact is maintained for subsequent ground contact.

Problems of Excess Plantarflexion and Dorsiflexion

Based on the studies done by Perry [8], excess plantarflexion and dorsiflexion normally occur in parallel with an abnormal pattern of contact between the foot and the floor. Excess plantarflexion occurs when an arc of more than 25 degree is formed between swing foot and ground during initial swing phase. Excess dorsiflexion occurs when an arc of more than 20 degree is formed between landing foot and ground during initial contact phase. Premature or delayed ankle lift due to abnormal postures results in deviation from the perfect landing. During single support period, excess plantarflexion on stance leg could disrupt rockers mechanisms which result in loss of progression. This implies a shorter step length and slower gait velocity. Also, the impairment of foot clearance and leg advancement during swing are the drawbacks of excess plantarflexion. Excess plantarflexion could be due to the initiation of extensor pattern during terminal swing phase. Excess dorsiflexion could reduce the shock absorption ability during initial contact phase. Subsequently, the body could not maintain an upright posture which in turn reduces the stability during mid-stance phase.

4.2.2 Mathematical Equations for Dorsiflexion and Plantarflexion

In this section, the mathematical equation for the ankle trajectory is further discussed. Based on the analysis in Section 4.2, the desired angular displacement of the ankle can be divided into three distinct segments during dorsiflexion. On the other hand, the desired angular displacement can be divided into four distinct segments during plantarflexion. In order to form a smooth and continuous function by linking each of this segment together, the following boundary conditions are applied on each segment, x.

Two boundary conditions from initial and final values:

$${}^{x}\boldsymbol{\theta}(\mathbf{0}) = \boldsymbol{\theta_0} \qquad {}^{x}\boldsymbol{\theta}({}^{x}\boldsymbol{t}) = \boldsymbol{\theta_f}$$

Also, two boundary conditions to ensure the function are continuous in terms of angular velocity:

$${}^{x}\dot{\boldsymbol{\theta}}(\mathbf{0}) = \dot{\boldsymbol{\theta}}_{\mathbf{0}} = {}^{x-1}\dot{\boldsymbol{\theta}}({}^{x-1}\boldsymbol{t}) \qquad {}^{x}\dot{\boldsymbol{\theta}}({}^{x}\boldsymbol{t}) = \dot{\boldsymbol{\theta}}_{\boldsymbol{f}} = {}^{x+1}\dot{\boldsymbol{\theta}}(\mathbf{0})$$

The initial ${}^{x}\boldsymbol{\theta}(\mathbf{0})$ and final ${}^{x}\boldsymbol{\theta}({}^{x}\boldsymbol{t})$ angular displacement of segment x have to be specified ($\boldsymbol{\theta_0}$ **and** $\boldsymbol{\theta_f}$) according to the dorsiflexion and plantarflexion landing pattern that discussed in Section 4.2. To ensure the continuity in terms of angular velocity, the initial angular velocity ${}^{x}\dot{\boldsymbol{\theta}}(\mathbf{0})$ for the current segment is equaled to the final angular velocity ${}^{x-1}\dot{\boldsymbol{\theta}}({}^{x-1}\boldsymbol{t})$ of the previous segment. Likewise, the final angular velocity ${}^{x}\dot{\boldsymbol{\theta}}({}^{x}\boldsymbol{t})$ of the current segment is equaled to the initial angular velocity ${}^{x+1}\dot{\boldsymbol{\theta}}(\mathbf{0})$ of the next segment. The via point velocity ($\dot{\boldsymbol{\theta}}_{\mathbf{0}}$ and $\dot{\boldsymbol{\theta}}_{\boldsymbol{f}}$) selection would be discussed in the later subsection. The notation ${}^{x}\boldsymbol{t}$ indicates the period for segment x. The initial angular velocity for the first segment and the final angular velocity for the last segment are set to be zero so that the landing pattern is continuous throughout the whole walking cycle. The four constraints can be satisfied by a polynomial equation of at least third degree. Generally, for each segment, a cubic polynomial with four coefficients is proposed as equation 3.4 below.

$$\theta(t) = a_0 + a_1 t + a_2 t^2 + a_3 t^3 \quad \text{---------- (3.4)}$$

The joint velocity and acceleration along the planned path are continuous as well.

$$\dot{\theta}(t) = a_1 + 2a_2 t + 3a_3 t^2 \qquad \ddot{\theta}(t) = 2a_2 + 6a_3 t \quad \text{---------- (3.5)}$$

Given the four constraints above, the coefficients of the cubic polynomial could be determined as equations 3.6 below.

$$a_0 = \theta_0$$

$$a_1 = \dot{\theta_0}$$

$$a_2 = \frac{3}{t_f^2}(\theta_f - \theta_0) - \frac{1}{t_f}\dot{\theta_f} - \frac{2}{t_f}\dot{\theta_0}$$

$$a_3 = \frac{-2}{t_f^3}(\theta_f - \theta_0) + \frac{1}{t_f^2}(\dot{\theta_f} + \dot{\theta_0}) \quad \text{---------- (3.6)}$$

Desired Velocities at the Via Points

In order to link all the segments in continuous manner, the desired velocity at the via points has to be specified. By assuming that all the via points are connected with straight line segments, zero velocity is assigned at the via points if the slope of these lines changes in sign at the via points. If the slope of these lines does not change sign at the via point, the average of the two slopes is chosen as the via velocity. By using this method, the velocity at the via point can be chosen solely based on the desired angular displacement at the via points.

Figure 4.5 indicates the desired angular displacement for supporting ankle during one walking cycle. The walking cycle is initiated through dorsiflexion followed by neutral position and then plantarflexion. Positive angular

displacement refers to dorsiflexion whereas negative angular displacement refers to plantarflexion. During plantarflexion, there are two via points at the sampling time of 20 and 30 respectively. During dorsiflexion, there are three via points at the sampling time of 69, 72 and 81 respectively.

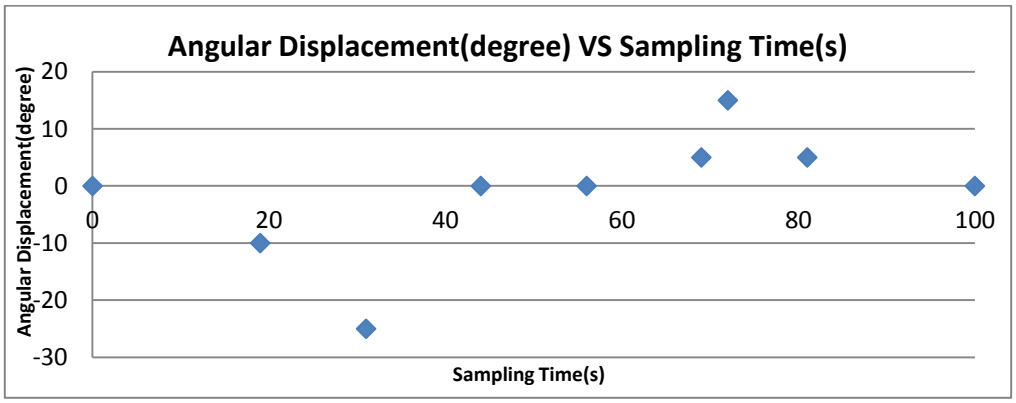

Figure 4.5: Desired angular displacement during one walking cycle

Given the dynamic constraint stated previously, the ankle trajectory at different phase can be formulated as equations 3.7 below:

$$\theta(t) = (-554.0249t^2 + 1458t^3) * \frac{\pi}{180} \qquad 0\ \% < t \leq 19\ \%$$

$$\theta(t) = (-10 - 88.815t - 1644.8t^2 + 11193t^3) * \frac{\pi}{180} \qquad 19\ \% < t \leq 31\ \%$$

$$\theta(t) = (-25 + 4437.9t^2 - 22758t^3) * \frac{\pi}{180} \qquad 31\ \% < t \leq 44\ \%$$

$$\theta(t) = 0 \qquad 44\ \% < t \leq 56\%$$

$$\theta(t) = (-1183.4t^2 + 11379t^3) * \frac{\pi}{180} \qquad 56\ \% < t \leq 69\%$$

$$\theta(t) = (5 + 269.3t + 15358t^2 - 441150t^3) * \frac{\pi}{180} \qquad 69\% < t \leq 72\%$$

$$\theta(t) = (15 - 2361.1t^2 + 13611t^3) * \frac{\pi}{180} \qquad 72\ \% < t \leq 81\%$$

$$\theta(t) = (5 - 63.89t + 246.9259t^2 - 257.2359t^3) * \frac{\pi}{180} \qquad 81\ \% < t \leq 100\%$$

---------- (3.7)

The notation t refers to walking cycle period in percentage.

The complete ankle trajectory is shown in Figure 4.6 below.

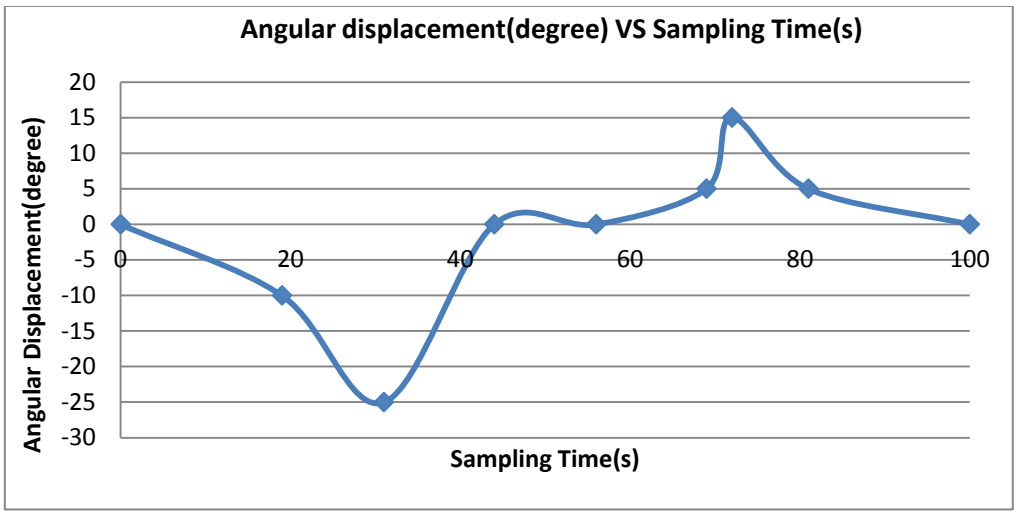

Figure 4.6: The ankle trajectory during one walking cycle

4.3 Comparison of Human Landing Pattern with Humanoid Robot Landing Pattern with the Proposed Foot System

In this section, dorsiflexion and plantarflexion landing pattern for human [8] and humanoid robot with the proposed foot system will be compared to justify the similarity between the two landing patterns.

The proposed foot system is designed such that it could absorb the landing impact as human foot. Also, the proposed foot system could ensure the ZMP of the humanoid robot is close to the center of the foot. Table 3.1 below summarizes the comparison of landing pattern between human and humanoid robot with the proposed foot system.

Table 4.1: Comparison of landing pattern behaviors between Human [8] **and Humanoid robot with the proposed foot system**

Walking Cycle	Human Foot	Proposed Foot
Initial Contact (0 % to 2 % walking cycle)	Ankle plantarflexion and ankle eversion are used to decelerate the landing impact.	Landing impact is converted to energy loss within the hydraulic fluid. It is used to enable the fluid exchange among the hydraulic cylinders
Loading Response (2% to 12% walking cycle)	Ankle plantarflexion is reduced during loading response phase.	Landing impact is distributed equally among the cylinders.
	The downward motion of the foot is slowed down when the pretibial muscle force is sufficient. This in turn enables the forefoot contact in quiet manner.	Extension and retraction of the cylinders act as damper systems which slow down the downward motion of the foot
	Rotation of the ankle is used to realign the joints axis so that it closer to the sagittal path of progression for the body.	Fluid exchanges via the Pascal's law are used to ensure the ZMP is maintained near to the centre of the foot.
	Some of the loading shock due to rapid limb loading is absorbed by pretibial and inverting muscles via ankle and foot mobility restriction.	When the ZMP is near to the center of the foot, the solenoid valves are locked and the fluids are directed to normally closed port that stopped by stoppers. This process reduces the loading impact to the stoppers.

Mid Stance (12% to 30% walking cycle)	Stable foot flat posture is provided via floor contact by the heel and the first and fifth metatarsal heads.	All the contact points stand firmly on the ground. ZMP is maintained at the center of the foot to ensure a stable foot posture.
	The normal balance between passive mobility and muscular control provide progression and stability.	Progression and stability are both served by the normal ZMP balance between passive fluid exchange and solenoid valves control.
Terminal Stance (31% to 50 % walking cycle)	Ankle joints are locked via eccentric active of the plantarflexor muscles.	Solenoid valves are used to lock the foot mechanism.
	The MTP joints are stabilized through the compressive force of the toe flexor muscles. The position of the ZMP is located between the first and second MTP joint.	Rubber pad on the proposed foot stabilizes the contact points. The ZMP is maintained at the centre of ankle.

Chapter 5: Hardware and Software Architecture

In this Chapter, the hardware and software components that contribute to the proposed foot design is discussed. The selection of the components is vital to prevent hydraulic fluid leakage and system failure.

5.1 Materials and Electronic Components Selection

Hydraulic cylinder, hydraulic oil, solenoid valves, force sensing resistor, arduino uno mircrocontroller, op-amp circuit and solenoid valve controller board make up the proposed foot system design. Each of the mentioned components would be discussed in the following section. Furthermore, Butterworth low-pass filter would be used to filter the signal from the force sensing resistor.

5.1.1 Hydraulic Cylinder

Figure 5.1: Hydraulic cylinder

Figure 5.1 indicates the selected hydraulic cylinder for the proposed foot system. A hydraulic cylinder is a mechanical actuator which could provide unidirectional force via unidirectional stroke when hydraulic power is supplied. In this study, the single acting hydraulic cylinders are selected.

Normally, pressurized hydraulic fluid is used as the power supply for the hydraulic cylinders. However, in this study, the pressure is generated from landing impact. Hence, hydraulic pump is not required for the proposed foot system. Landing impact could provide fixed or regulated fluid flow to ensure

fluid exchange among the four cylinders. The extension and retraction of the hydraulic cylinder are based on Pascal's law. Hence, the system could be regarded as a proactive system.

Theoretical Push and Pull Forces

To simplify the determination of push and pull forces, it is assumed fluid pressure is not exerted in the piston rod. Hence, as shown in equation 5.1, the force *F* on the piston rod can be determined through the multiplication of the pressure *P* in the cylinder times the piston area *A*:

$$F = P \cdot A \quad \text{---------- (5.1)}$$

Where F refers to the impact force in Newton, P indicates the pressure inside the cylinder in Pascal and A is the effective area of cylinder piston in square meter.

Hydraulic Cylinder Selection

The hydraulic cylinder with a bore size of 25mm and stroke of 25mm is selected to serve the foot system design purpose. Stroke of 25 mm is selected as it is difficult for bipedal robot to walk stably on uneven terrain with 20 mm fluctuations even when a real-time stability controller is implemented. The extra 5mm serves for safety and tolerance purposes. A bore size of 25 is chosen such that the pressure of the hydraulic fluid in the cylinder is not too high and the fluid exchange is guaranteed. High pressure may result in hydraulic fluid leakage. Also, since the weight of the cylinder is proportional to the bore size of the cylinder, bore size of 25 mm is chosen such that the proposed foot system is light and compact. For the proposed foot system, since the weight of the testing bipedal robot is 65 kg, the pressure in the hydraulic system during static standing can be determined as follow:

$$Pressure = \frac{weight * gravity\ constant}{\pi r^2} = \frac{65 * 9.81}{\pi * (0.0125)^2} = 1.359MPa$$

Hence, the connecting tube, t-tube, connector, silencer and the solenoid valves selected should be at least sustaining the calculated pressure. In order to ensure the hydraulic system is not subjected to fluid leakage, the author selected the component that can at least sustain 2 times the determined pressure. This is because a very high impact will be exerted onto the four contacts points during landing. The impact is random and could not be determined easily. Hence, in order to ensure the system could absorb the impact, the components selected are based on the safety pressure of 2.6Mpa.

Advantages of Using Hydraulic Cylinders

Hydraulic cylinders could play the role as dampers which resist motion via viscous friction. The dampers could be used to supress or absorb shock impact and dissipate kinetic energy. Landing impact is converted to fluid friction and the energy to move the stroke of the hydraulic cylinder. Fluid friction is due to the flow of fluid via a narrow orifice and it is converted to heat inside the viscous fluid. Hence, the hydraulic fluid selected should have high heat capacity. Fluid friction is proportional to the translational velocity of the stroke but it acts in the opposite direction of the stroke movement. Subsequently, the stroke movement is slow down and the landing impact is absorbed.

5.1.2 Solenoid Valve

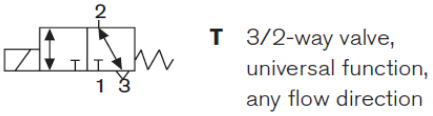

Figure 5.2: 3/2 ways solenoids valve

Figure 5.2 shows the selected solenoid valve for the proposed foot system. It is used to control the fluid exchange among the cylinders. A solenoid valve has two functional units which are solenoid operator and valve body. Solenoid operator is used to switch the fluid flow direction. Valve body is used to stop

the fluid flow. A solenoid valve could be regarded as a large inductor which consists of a coil of wire with a magnetic core. As a current is moving in the solenoid, the inductance would move that current continuously. Hence, a large voltage across solenoid leads would be created when the solenoid is switched off. The current arc due to this large voltage would either be moved through the air or burn through a semiconductor. In order to prevent the mentioned problems, the energy stored in the solenoid magnetic fields must be dissipated by providing an easy and safe path for the current flow. Hence, a diode is connected in serial with the solenoid to prevent the large voltage generated.

Solenoid Valve Selection

Given the limiting pressure above, the solenoid valves are selected such that they can open and close the valve under differential pressure of at least 2.6 MPa. The on-off state of the solenoid is controlled by using Arduino UNO microcontroller board through PWM signal.

Solenoid Valve Control Circuit

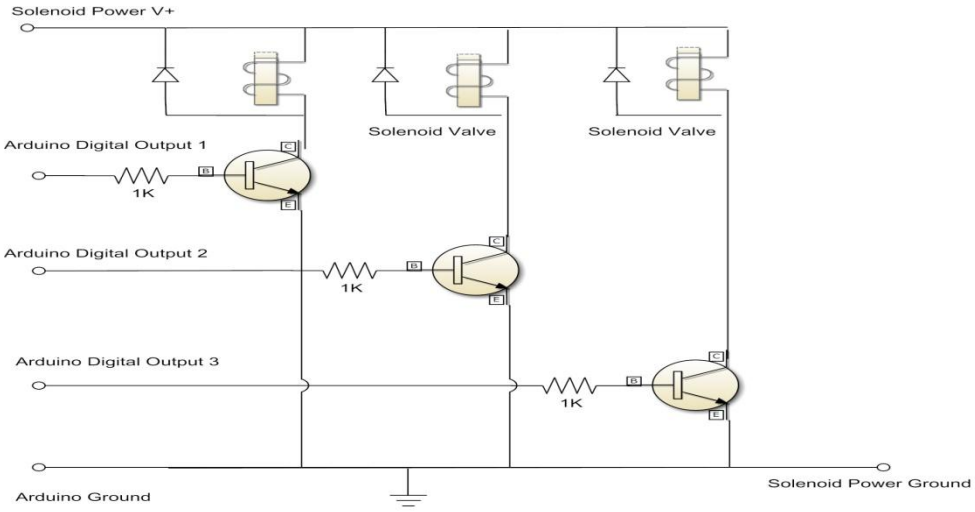

Figure 5.3: Solenoid valves control circuit

The solenoid control circuit is shown in Figure 5.3 above. A NPN transistor or field effect transistor is used to provide sufficient current to the solenoids.

Also, the transistor can be used as a switch. The Collector is set to be higher voltage than the Emitter by connecting the Emitter to ground. As the Base (B) of the transistor is remained low in current, the Collector would be disconnected from the Emitter. The solenoid circuit is in the “unlocking” state. When the Arduino UNO controller provides a 5v signal to the Base, the transistor would connect the Collector and Emitter together which in turn close the solenoid circuit for “locking” state. The voltage at the Base should not set in between 0 to 5V because it can conduct partially and dissipate a lot of heat energy.

Transistor Selection

The product of the current from Arduino UNO controller (40mA) and the current gain of the transistor (hfe) have to be larger than the current required by the selected solenoid. This setting is to ensure the transistor in saturated state. For safety purpose, this product magnitude should be two times larger than the current required by the solenoid valve selected. The resistor that connected to the transistor is used to modulate appropriate current to the transistor. Any resistor with resistance 1k or below is suitable for this application. However, the lower resistance would result in the more current consumption to turn on the transistor.

Bypass Diode Selection

Generally, the diode selected connects the power source through the ground of solenoid valve with the Collector of transistor to prevent the back emf of solenoid from damaging the circuit. The diode selected would not be conducted when the solenoid in on or idle state. Since the solenoid valve is an inductor, a back flow current would be generated when the solenoid is turned off. This current would be directed through the diode until the energy is dissipated. Subsequently, the voltage could be harmlessly redirected back into the solenoid to prevent any damage to rest of the circuit. This diode should

have a reverse breakdown voltage of at least equals to the power supply voltage and capable of redirecting the current that flows through the solenoid valve. Figure 5.4 below indicates the real solenoid valve control circuit with the electronic components selected above.

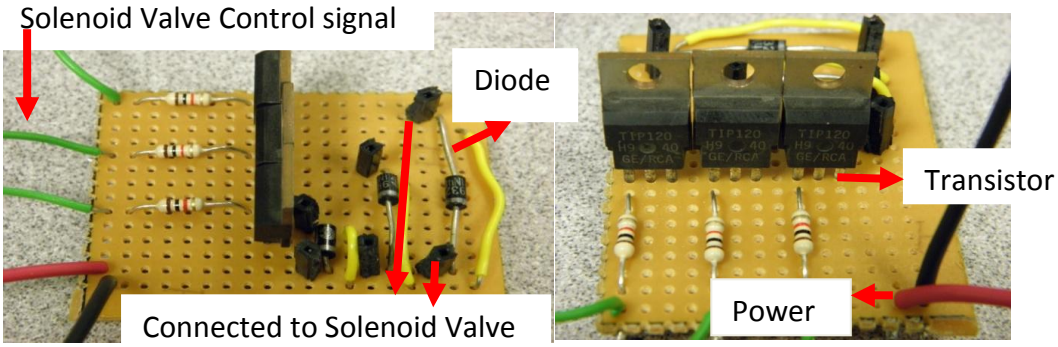

Figure 5.4: Solenoid valves electronic circuit

5.1.3 Force Sensing Resistor (FSR)

Figure 5.5: Force Sensing Resistor

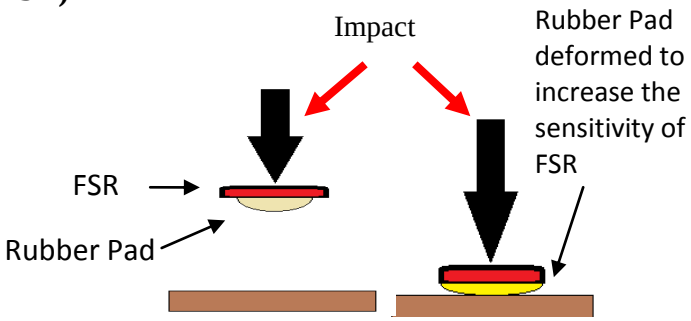

Figure 5.6: Mechanism to increase the Sensitivity of FSR

Figure 5.5 above indicates the selected force sensing resistor (FSR) for the proposed foot system. It is used to detect the landing state. FSR is made by polymer thick film (PTF) that has a thickness of about several Pico meter. This material is robust and hard to have physical deformation which is suitable to sustain the landing impact. As the applied force on the active surface of FSR increases, the resistance of the FSR would be decreased. The change in

resistance could provide analog signal. FSR is not suitable for accurate force measurement because it has an error rating of about 5% to 25%. Nonetheless, for the measurement of ZMP, the precision issue could be neglected since only the ratio of the force applied to each FSR is interested.

In order to increase the sensitivity of the FSR, a rubber pad has been attached to each FSR. Via this attachment, the force exerted on the rubber would be equally distributed onto the contact surface of the FSR. This mechanism is shown in Figure 5.6 above. Besides adding a rubber pad, a frictional pad is attached to the FSR as well. This frictional pad is added so that slippage on the contact point could be prevented when landing on the contact surface. Slippage might result in improper landing.

Op- Amp Circuit

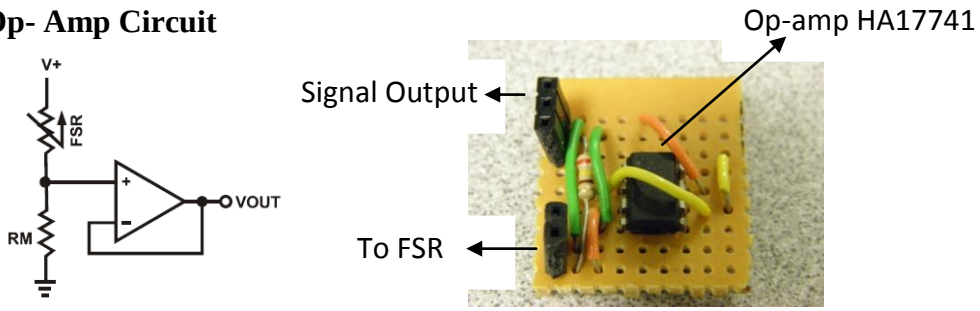

Figure 5.7: Op-amp circuit

The op-amp circuit for the FSR is shown in Figure 5.7 above. A general purpose 741 op-amp is used to increase the sensitivity of the FSR. The selection of the gain value would be discussed in the following section.

FSR Voltage Divider

The FSR is connected to a known resistor in a voltage divider configuration to achieve a simple force-to-voltage conversion [5]. The output from the amplifier can be determined via the equation 5.1 below.

$$V_{out} = \frac{V_+}{1+\frac{RFSR}{RM}} \quad \text{------ (5.2)}$$

In Figure 5.7, the output voltage would increase with increasing force. The reference resistor, RM, is chosen such that it maximizes the force sensitivity in the desired range. Also, it is used to limit current flow through the FSR. The current through the FSR should be limited to less than 1 mA/square cm of applied force. This configuration could maintain low bias currents which would reduce the error due to the source impedance of the voltage divider.

Op-amp Selection

The selected HA17741/PS op-amp is a high-performance operational amplifier that equipped with internal phase compensation. Figure 5.9 shows the selected op-amp HA17741.

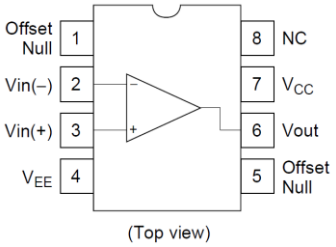

Figure 5.8: Op-amp HA17741 [5]

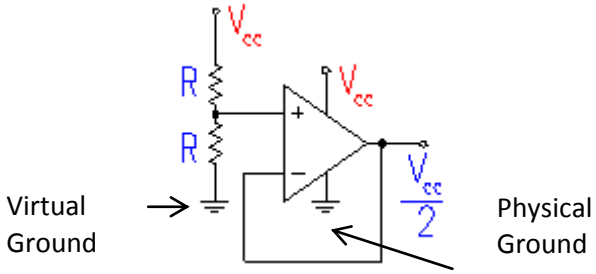

Figure 5.9: Single Supply Op Amps [5]

Single Supply Op-Amp

Since the Arduino controller could only take in positive analog output from the sensor, the designed amplifier has to be a single supply op-amp (V_{cc} negative is connected to ground). This configuration is named as rail-to-rail op amps because it could provide output voltage that closed to the power supply voltages (or rails).

Virtual Ground

Virtual ground is a voltage reference that is used to complement the circuit that does not required negative output [5]. A virtual ground configuration is shown in Figure 5.9. The non-inverting input to the op-amp can be set to half

of Vcc via voltage divider formed from the two resistors. The output of the op-amp is half of Vcc as well since it is set up as a follower. This configuration provides noise reducing ability. The op-amp should be used in its inverting configuration which does not require ground current.

5.1.4 Aduino UNO Microcontroller

Figure 5.10 shows the selected Aduino UNO microcontroller. It is used to take in FSR input and control the on-off state of the solenoid valves accordingly.

Figure 5.10: Aduino UNO microcontroller

The Arduino Uno is a microcontroller which has 14 digital inputs or output pins (of which 6 can be used as PWM outputs), 6 channels 10-bit analog to digital converter and a 16 MHz crystal oscillator. The analog to digital converter (ADC) maps input voltages between 0 and 5 volts into integer values between 0 and 1023. This mapping provides a resolution of 5 volts per 1024 units or 4.9 mV per unit. Hence, the minimum analog input is 4.9mV. The overall sample rate determined by the serial data rate. In order to record the compromised real time FSR inputs and control the solenoid valves instantaneously, the baud rate is set to be 38400 baud. Given this baud rate, there is about 400 data would be recorded in one second. Thus, the sampling period that used in this study is 0.0025seconds.

5.1.5 Foot Plate

The foot plate is made of aluminum material which is light weight and could provide higher modulus of elasticity. This characteristic is vital to develop a rigid foot system. If the foot plate is easily subjected to bending, the ZMP would not be remained at the center of the foot even the Bang-Bang controller is applied. In order to prevent bending along pitch axis, the thickness of the footplate is set to be 3mm. This thickness parameter is determined via finite element analysis.

5.1.6 Hydraulic Oil Selection

The functions of hydraulic oil are power transmission, system components lubrication, and heat absorption. Viscosity is the most important element in selecting the hydraulic oil as the fluid is used as the power transmission medium. High viscosity would increase internal fluid frictions which in turn reduce the fluid flow rate. Boundary lubrication may be triggered at the solenoid valves. Low viscosity might increase internal and external leakage which would result in power transmission reduction and overall pressure loss within the system. Low viscosity hydraulic oil (SAE viscosity grade 20 oil) is selected to ensure fast and smooth fluid exchange inside the hydraulic cylinders. The benefits of using SAE viscosity grade 20 oil include longer service life, forming resistance, chemically stable and lower maintenance cost. Hydraulic fluid selected must be compatible with tube and seal materials.

5.2 Second-order Butterworth Low-pass Filter

The FSR signals are acquired through a 10-bit-resolution ADC with a sampling rate time 0.0025s. The force measurements are noisy and the FSR are sensitive to vibrations during walking motion. Noise and high frequency vibrations from the FSR signals could be minimized via the second-order Butterworth low-pass filter [51]. The second-order Butterworth low-pass filter is a signal processing filter which is designed to generate an approximately flat

frequency response in the pass band [51]. It is also referred to as a maximally flat magnitude filter. The second-order Butterworth low-pass filter does not reject the unwanted frequencies completely but reserve uniform sensitivity for the wanted frequencies as possible. The second-order Butterworth low-pass filter is selected as it could provide the ability of smoother signal output generation, short-term fluctuations removal and longer-term trend maintenance.

The second-order filter has significance ability to attenuate higher frequencies. This is important to filter out vibration noise when the bipedal robot is landing on swinging foot. Via the second-order Butterworth low-pass filter, the signal amplitude could be reduced to one fourth of its original magnitude every time as the frequency doubles. The actual amount of attenuation for each frequency could be tuned via experimental testing and observation when the bipedal robot is walking. The delay of the signal output should be less than 6ms.

The difference equation for a second-order Butterworth low-pass filter [51] with unity gain can be expressed as equation 5.3 below.

$$y(n) = b(x(n) + 2 * x(n-1) + x(n-2)) - a_2 y(n-1) - a_3 y(n-2) \text{---- (5.3)}$$

$$\mathrm{b} = \frac{oc^2}{base}$$

$$a_2 = \frac{(2 * oc^2) - 8}{base} \qquad a_3 = \frac{4 - 2\sqrt{2} * \mathrm{oc} + oc^2}{base}$$

$$oc = 2tan(\pi * cutoff * period) \qquad \mathrm{base} = 4 + 2\sqrt{2} * \mathrm{oc} + oc^2$$

Where y refers to the filtered variable, x indicates the unfiltered variable, x (n) is the value of x at time t (n), y (n) is the value of y at time t (n), t (n) = (n * T) is the current time, T = t (n) – t (n−1) is the constant sampling interval, n is an integer and $cutoff$ refers to cut-off frequency.

Chapter 6: Walking Test Evaluation

In this chapter, the walking test experimental results would be discussed to justify the feasibility of the proposed foot system design. ZMP criterion would be used to compare the walking stability for the case with and without the proposed foot system.

6.1 Walking Test Consideration

Before the start of walking test, the proposed foot system should be maintained at levelled position so that the motion is started at stable position. In other words, the bipedal robot has to standing on ready to walk position for a while so that the fluid exchange could be triggered and achieve levelled position automatically. Levelled position implies that the ZMP is close to the centre of each foot. This position could be verified by using spirit level.

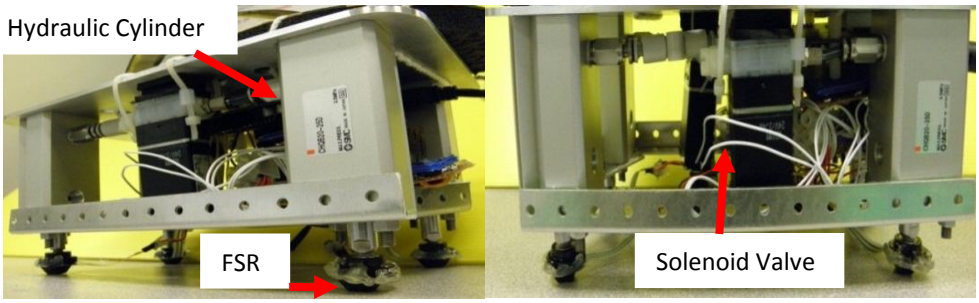

Isometric View Side View

Figure 6.1: Assembly of the Proposed Foot

Table 6.1: Specifications of the proposed foot

Height	78mm
Length	140mm
Width	240mm
Stroke	250 mm
Weight	1.6kg

Figure 6.1 above shows the assembly of the proposed foot system. Table 6.1 summarizes the specifications of the proposed foot.

6.2 Experimental Tests

The proposed foot system is designed such that it has high applicability. It can be applied to all bipedal robots. In order to justify the feasibility and the functionality of the proposed foot system, the ZMP stability criterion is chosen as the necessary stability indicator. This criterion imposes the constraint that the ZMP must be situated inside the foot support polygon. ZMP is not an absolute stability condition but a necessary constraint which ensures the foot does not rotate along one of its edges and free of slippage. As the ZMP is close to the center of the support polygon, the stability margin would become larger which could provide higher stability to the bipedal robot. The stability margin [36] can be defined as the minimum distance between the ZMP and the boundary of the support polygon (Figure 6.2). Hence, stability margin can be used as the stability evaluation function for bipedal robot.

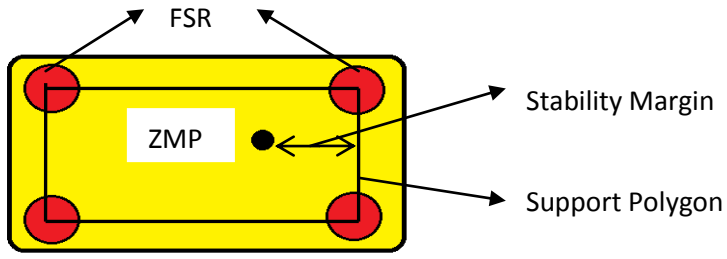

Figure 6.2: Stable region and stability

Then, given the criteria, the four different experiments have been conducted as follows:

a) Comparison of ZMP criteria when the robot is walking on the spot with and without the new proposed foot.
b) Comparison of ZMP criteria when the robot is walking forward with and without the new proposed foot.
c) Comparison of ZMP criteria when the robot is walking on a raised platform with and without the new proposed foot.

d) Comparison of ZMP criteria when the robot is walking on a slope (7 degree) with and without the new proposed foot.

Besides, in order to have better comparison, the concept the Sum of Squares for Error (SSE) is utilised. It is used to measure the difference between the collected data with a desired model or trajectory [31]. In this study, it is used to assess how well the ZMP fits to the reference or desired ZMP. Mathematically, SSE can be defined as the sum of the squared differences between each data and the mean of data set [31]. It identifies the variation within a data set. The SSE would produce a null magnitude if all the data within a data set are identical. A small SSE indicates a close fit of the model to the data. The SSE can be expressed via the equation 6.1 below.

$$SSE = \sum_{i=1}^{n}(x_i - \bar{x})^2 \qquad \text{---------- (6.1)}$$

Where n is the number of data, x_i is the value of the ith data and $\bar{x}$ is the mean of all the data set. In this study, the mean refers to the reference ZMP.

The proposed foot was tested on ASLAN which is a life-sized humanoid robot. The step time for the robot is 1 step per second. The step length is set for different magnitude for different walking tests. Through the experiments, the effectiveness of this foot system was confirmed.

Comparison of ZMP criteria when the robot is walking on the spot motion with and without the new proposed foot

On the spot walking motion is the most important walking motion that contributes to the omni-directional motion of the bipedal robot. This is because it is the starting point of walking motion in 3D plane. This experiment is used to compare the performance of walking on the spot motion for the case with and without the proposed foot.

Figure 6.3 and Figure 6.4 below show the variation of Xzmp(mm) and Yzmp(mm) of the bipedal robot respectively when the robot was walking on the spot for three consecutive walking cycle. The walking cycle ended within 8 s. The ZMP variation was started when the robot was in the single support phase where right leg was being lifted up. The walking motion ended when the right foot finished single support phase and entered double support phase.

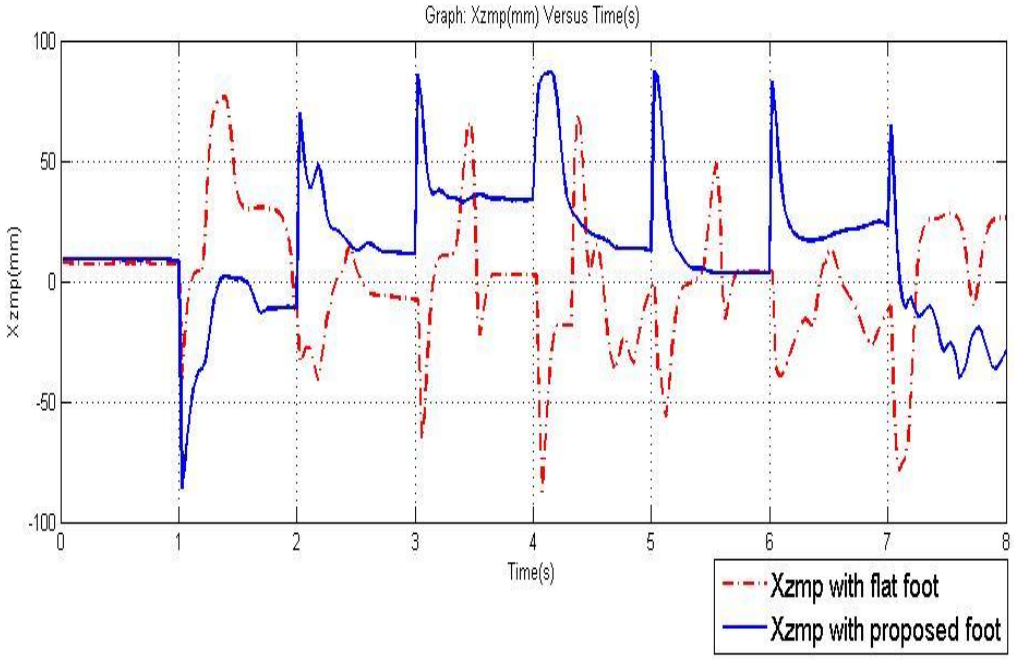

Figure 6.3: The variation of X_{zmp}(mm) for on the spot motion(with and without the proposed foot)

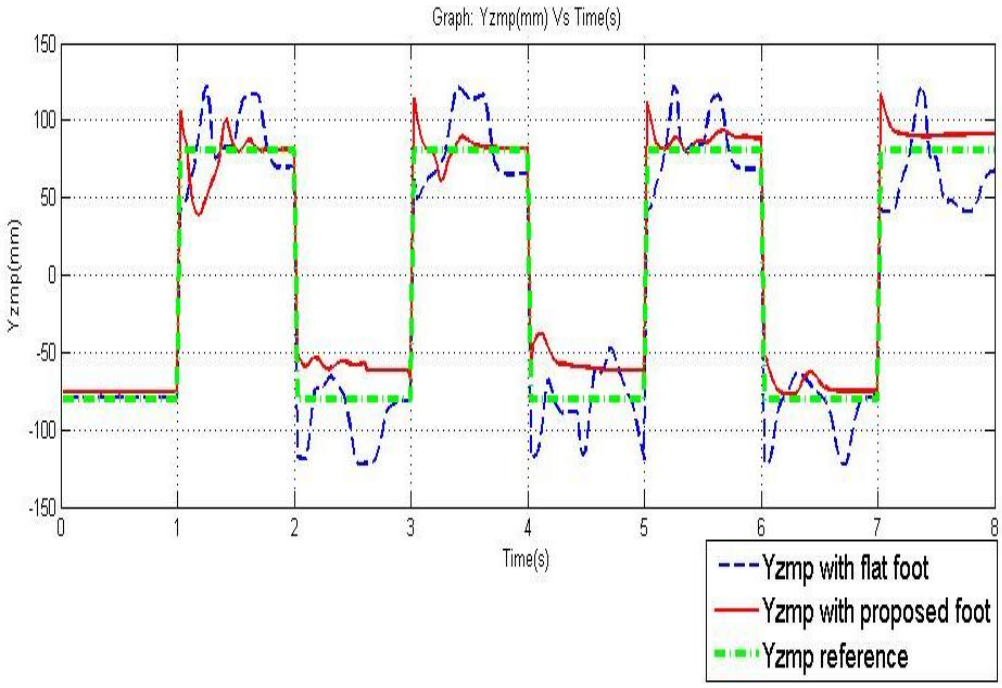

Figure 6.4: The variation of Y_{zmp} (mm) for on the spot motion (with and without the proposed foot)

Based on Figure 6.3and 6.4, the Xzmp and Yzmp of the testing robot are close to the reference ZMP when it was equipped with the proposed foot system. The robot required at most 0.5s to enter steady state [42]. In steady state, the ZMP should be remained unchanged or subjected to small variation with respect to the steady ZMP (±10% error) [42].The short period before the steady state is termed as transient state [42]. In transient state, the variation of Xzmp and Yzmp might be due to the fluid exchange in the hydraulic cylinders where the foot is locating the desired ZMP. The steady ZMP on supporting foot is vital to prepare a firm foundation for swinging foot during single support phase. Also, the steady value implies that the walking motion was subjected to less 'vibration' due to the damper effect of the hydraulic system.

For the case with flat and rigid foot, although the variation of ZMP is close to the reference ZMP, there were some fluctuations and the steady state was relatively shorter. Hence, the walking motion was subjected to 'vibration'. The

variation of the ZMP (in closer view) on the foot is shown via Figure A and B in Appendix 1. Through these two Figures, it is clear that the ZMP was maintained near the centre of the foot when the testing robot with the proposed foot was walking on the spot. In order to quantify how well the ZMP fits to the reference ZMP, table 6.2 tabulates the mean SSE for Xzmp and Yzmp respectively during on the spot walking motion for the case with and without the proposed foot system. Based on table 6.2, the mean SSE of Xzmp and Yzmp are smaller for the case with the proposed foot. This implies that the ZMP for the case with the proposed foot are closer to the reference ZMP.

Table 6.2: Comparison of mean SSE for the case with and without the proposed foot during on the spot walking motion

Mean SSE	With Proposed Foot	Without Proposed Foot
Xzmp	0.01850	0.03273
Yzmp	0.00967	0.02190

Comparison of ZMP criteria when the robot is walking forward with and without the new proposed foot

This experiment is used to compare the performance of walking forward motion for the case with and without the proposed foot. The bipedal robot was walking at a pace of 1step per second. Equipped with the proposed foot, the bipedal robot could walk at a faster velocity (3cm/step). On the other, the maximum walking velocity for the case of flat foot is 2cm/step with the same step period. The improvement of the walking velocity might be due to the damping effect on the proposed foot where the landing impact is reduced and the ZMP is strictly kept near to the centre of the foot.

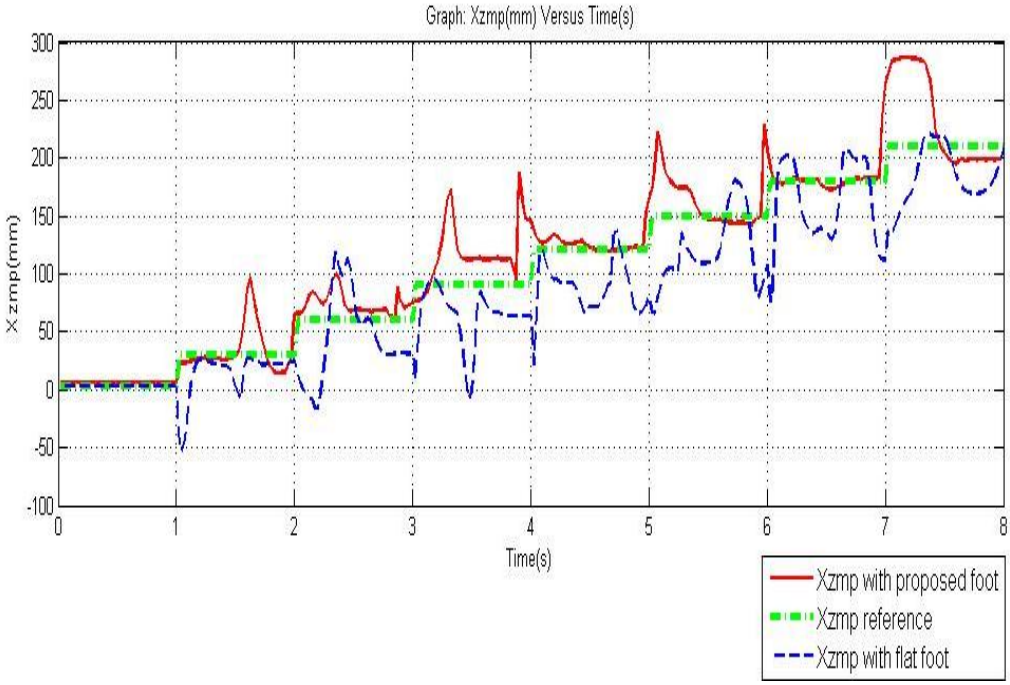

Figure 6.5: The variation of Xzmp(mm) when the robot is walking forward(with and without the proposed foot)

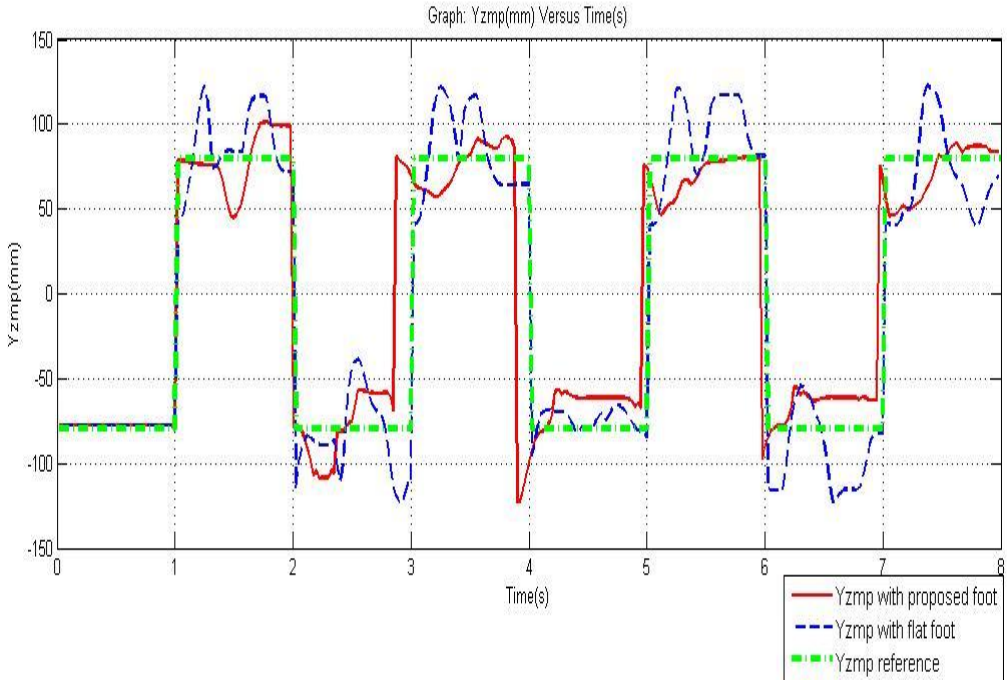

Figure 6.6: The variation of Yzmp(mm) when the robot is walking forward(with and without the proposed foot)

Figure 6.5 and 6.6 show the variation of Xzmp and Yzmp respectively when the robot is walking forward for three consecutive walking cycles. Based on the graph above, the Xzmp and Yzmp of the bipedal robot with the proposed foot system were maintained near to the reference ZMP. This implies that the bipedal robot with the proposed foot has achieved higher walking stability. Also, during single support phase, the variation of ZMP was less for the case with the proposed foot. During each walking step, the bipedal robot with proposed foot system required at most 0.5s to enter the steady state. The bipedal robot required more time (as compared to on the spot walking motion) to enter the steady state because the COM of the robot was moving in sagittal plane as well. In the steady state, the Xzmp and Yzmp were maintained at the centre of the supporting ankle until the end of single support period of the swinging leg. This is vital to prepare a stable foundation for the swinging leg. The steady ZMP value implies that the walking motion was subjected to less 'vibration'. The variation of the ZMP (in closer view) on the foot is shown via Figure E and F in Appendix 1. Through these two figures, it is clear that the ZMP was maintained near to the centre of the foot when the testing robot with the proposed foot was walking forward.

In order to quantify how well the ZMP fits to the reference ZMP, table 6.3 tabulates the mean SSE for Xzmp and Yzmp respectively. Based on table 6.3 the SSE for Xzmp and Yzmp are smaller for the case with the proposed foot system. This implies that the ZMP for the case with the proposed foot are closer to the reference ZMP as compared with the case of flat foot.

Table 6.3: Comparison of mean SSE for the case with and without the proposed foot during walking forward motion

Mean SSE	With Proposed Foot	Without Proposed Foot
Xzmp	0.02518	0.05602
Yzmp	0.02335	0.05948

Comparison of ZMP criteria when the robot is walking on a raised platform with and without the new proposed foot

This experiment is used to compare the performance of walking motion on a raised platform for the case with and without the proposed foot. Also, this experiment is used to justify that the stabilization of the proposed foot system is in 2 dimensions which referred to the pitch and roll axes with respect to the testing robot. This is done by letting the left leg of the testing robot to walk along the edge of the raised platform. Also, two different types of landing patterns are compared in this experiment. This is to show that the landing pattern would facilitate the adaptability of the proposed foot.

Equipped with the proposed foot, the robot could walk on the raised platform but with a slower speed (2cm/step) at the pace of 1 step per second. On the other hand, for the case with flat foot, the robot would fall when it stepped on the raised platform.

For flat foot landing pattern, the testing robot with the proposed foot is able to walk on a raised platform with the height of 10 mm only. In order to further increase the ability to adapt to higher raised platform, the landing pattern with dorsiflexion and plantarflexion is utilised. This landing pattern is discussed in Chapter 4. With this kind of landing pattern and the proposed foot, the testing robot is able to walk on a raised platform with the height of 15mm.

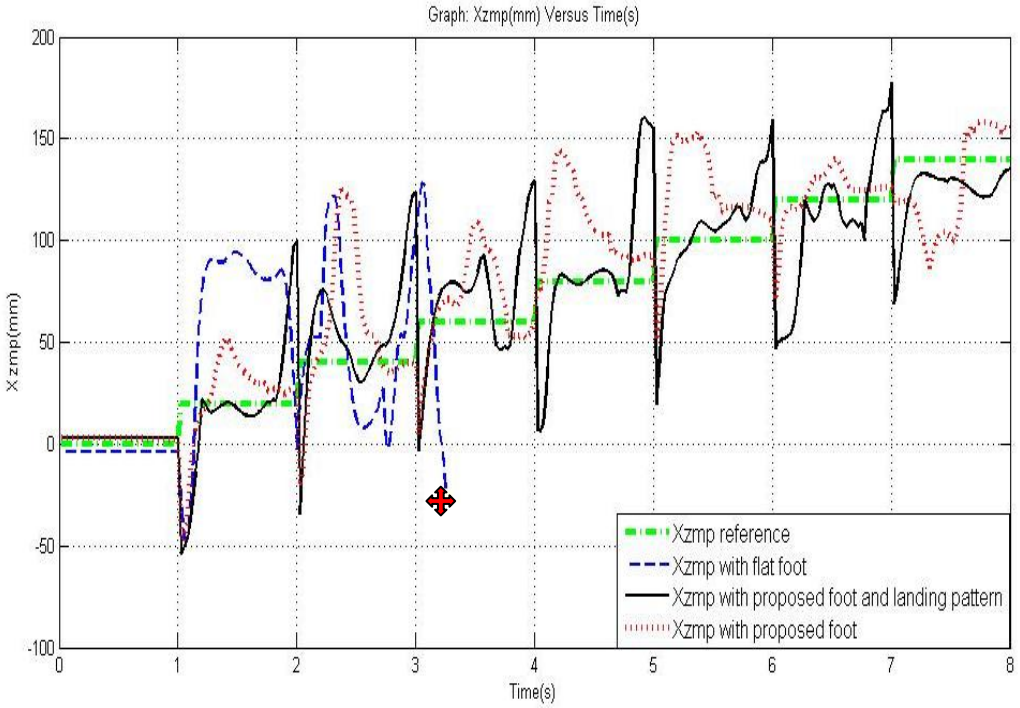

Figure 6.7: The variation of Xzmp(mm) when the robot is walking on a raised platform (with and without the proposed foot)

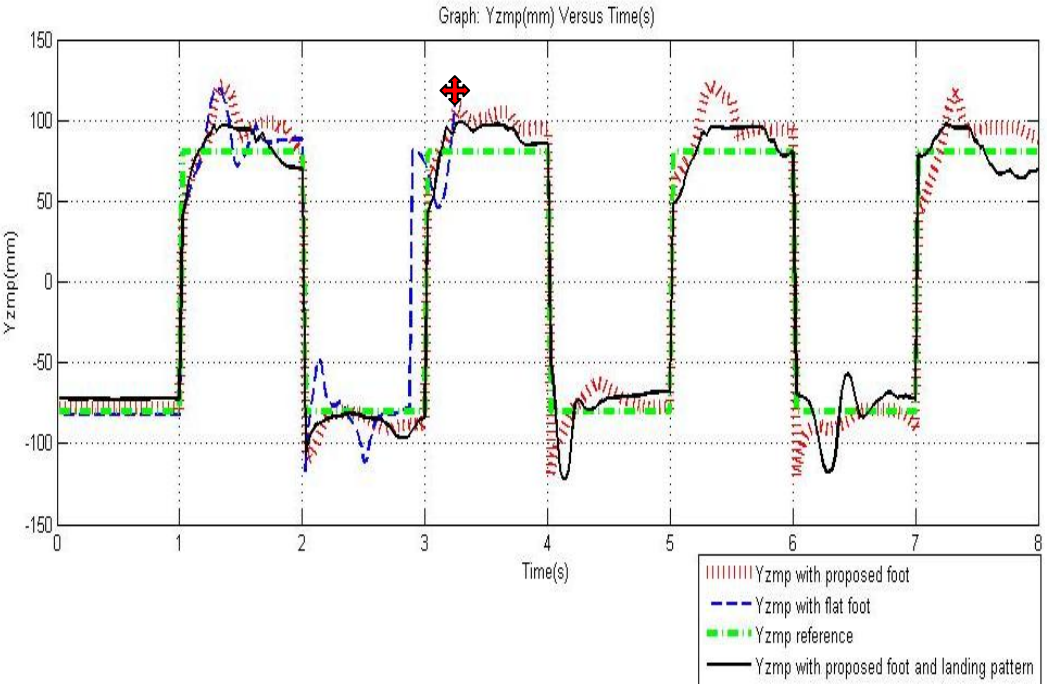

Figure 6.8: The variation of Yzmp(mm) when the robot is walking on a raised platform (with and without the proposed foot)

Figure 6.7 and 6.8 show the variation of Xzmp and Yzmp respectively when the robot was walking on the raised platform for three consecutive walking cycles. Based on the graph above, the Xzmp and Yzmp of the robot with the proposed foot are maintained near to the ZMP reference. This implies that the robot with the proposed foot has achieved higher walking stability. Also, during each single support phase, the variation of ZMP is less for the case with the proposed foot.

For the case with flat foot, the robot fell backward at the time of 3.3s (marked as a red cross in Figures 6.7 and 6.8 respectively). For the case with proposed foot, the robot required at most 30 sampling time unit (0.6s) to enter the steady state. Besides moving in sagittal plane, the robot has to adapt to the raised platform along Z-axis and unevenness in lateral plane. Hence, more time (as compared to walking forward motion) are required to reach the steady state. In the steady state, Xzmp and Yzmp were maintained at a steady value until the end of single support phase. The steady ZMP value implies that the walking motion is subjected to less 'vibration'. For the case with dorsiflexion and plantarflexion landing pattern, the testing robot landed at the heel and then moved the Xzmp to the center of the ankle during double support phase. There was an immediate but brief peak in the ZMP pattern and it is termed as heel strike transient (HST) [8]. The Yzmp on the supporting ankle was maintained at the centre (on the supporting foot) until the end of single support period. At the end of double support period, the supporting ankle (behaves as swinging leg for the next walking cycle) implemented plantarflexion to generate foot rocker for the progression of next walking cycle. In order to quantify how well the ZMP fits to the reference ZMP, table 6.4 tabulates the mean SSE for X_{zmp} and Y_{zmp} respectively when the robot is walking on a raised platform with the height of 10 mm. The case with landing pattern of dorsiflexion and plantarflexion is not compared as this landing pattern is not designed to fit the reference ZMP. This landing pattern is used to control the movement of ZMP such that it is moved with constant velocity and maintained near to the centre

of the supporting ankle during steady state. Based on table 6.4, the mean SSE for X_{zmp} and Y_{zmp} are smaller for the case with the proposed foot. This implies that the ZMP for the case with the proposed foot are closer to the reference ZMP.

Table 6.4: Comparison of mean SSE for the case with and without the proposed foot during walking on a raised platform (10mm height)

Mean SSE	With Proposed Foot	Without Proposed Foot
Xzmp	0.03209	0.16240
Yzmp	0.01045	0.06951

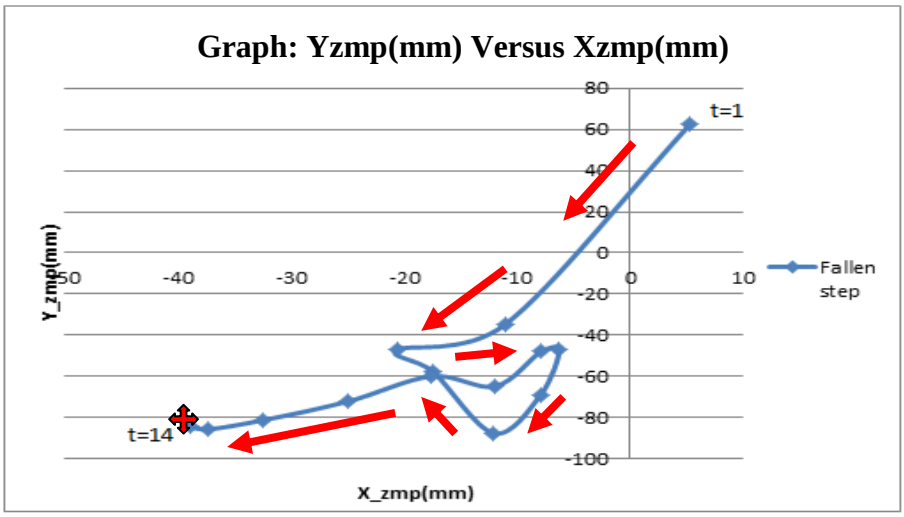

Figure 6.9: The variation of ZMP when the flat foot robot started to walk on a raised platform with a height of 15mm.

To magnify the movement of ZMP on the foot during falling step, figure 6.9 shows the variation of ZMP when the robot with flat foot started to walk on a raised platform with a height of 10mm. The red arrow indicates the movement of ZMP on the left foot (the step that triggered falling). At the sampling time of 14, the ZMP moved quickly to the bottom edge of left foot. Subsequently, the robot fell (toppled) to the left hand side. The red cross in Figure 6.9 indicates the falling state. This result indicates that the robot with flat foot is unable to maintain the ZMP in the support polygon of the foot. On the other

hand, the variation of the ZMP (in closer view) on the proposed foot system is shown via Figure I and J in Appendix 1. Through these two figures, it is clear that the ZMP could be maintained near to the centre of the foot when the testing robot with the proposed foot was walking on the raised platform.

Figures 6.10 and Figure 6.11 show the adaptability of the proposed foot on a raised platform of 10mm and 15mm height respectively.

Snapshots for Walking on a Raised Platform with a Height of 10mm

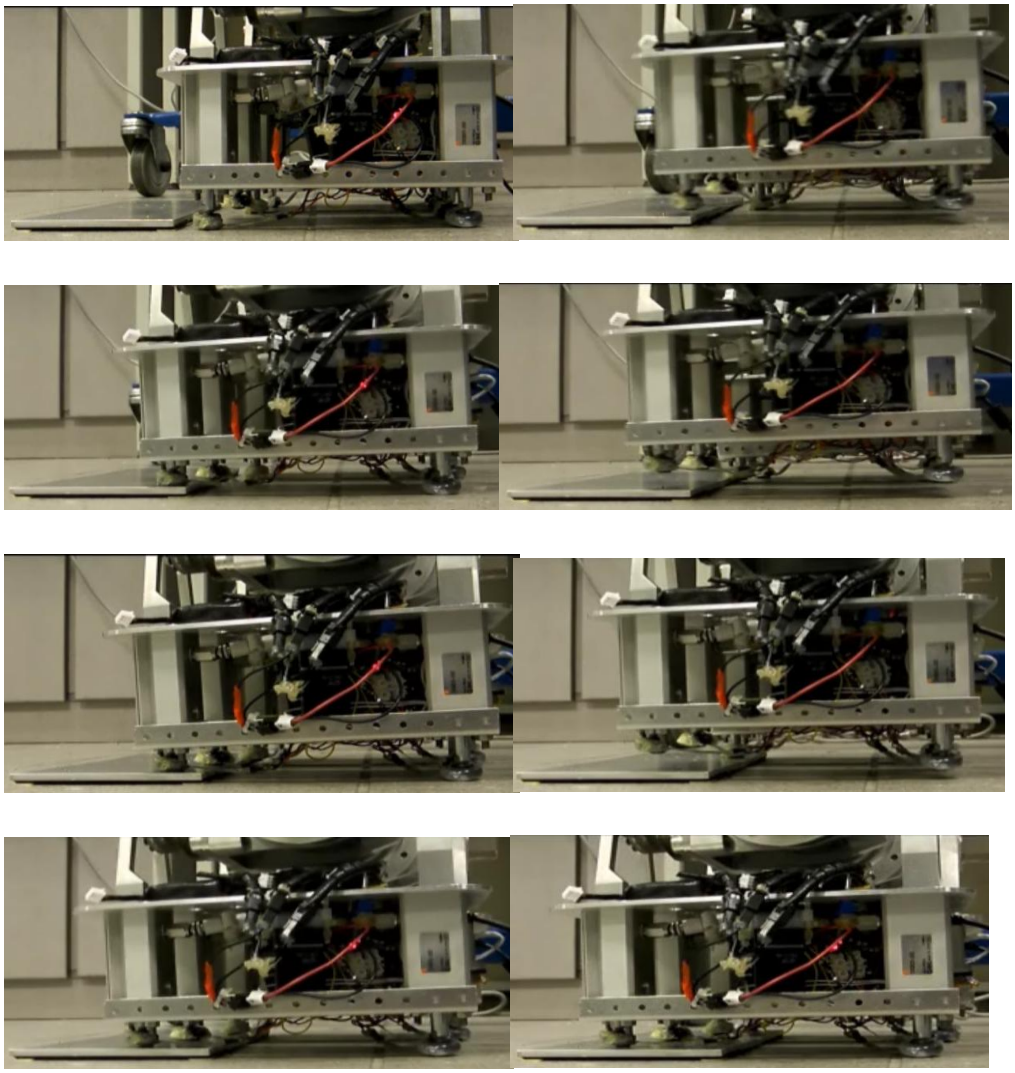

Figure 6.10: Snapshots for walking on a raised platform with a height of 10mm

Snapshots for Walking on a raised platform with a Height of 15mm (dorsiflexion and plantarflexion landing pattern)

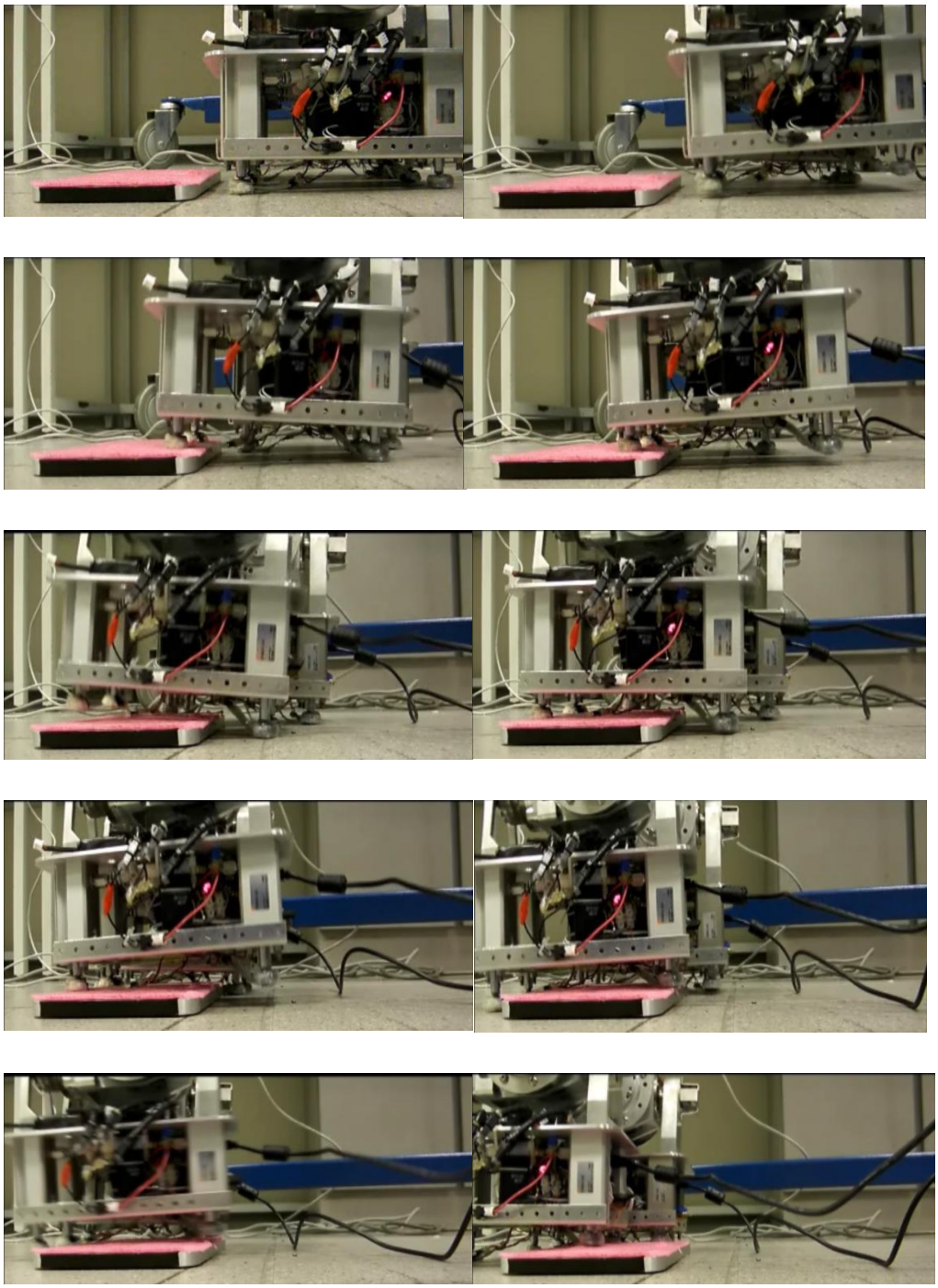

Figure 6.11: Snapshots for walking on a raised platform with a height of 15mm

Comparison of ZMP criteria when the robot is walking on a slope (7 degree) motion with and without the new proposed foot

Theoretically, given the maximum stroke of the cylinder and the length of the foot, the robot with the proposed foot system should be able to adapt to a slope with a maximum gradient of 8 degree. However, in the real situation, the robot could only walk stably on a slope with gradient of 7 degree. Equipped with the proposed foot, the robot could walk at a speed of 30mm/step on the slope without falling.

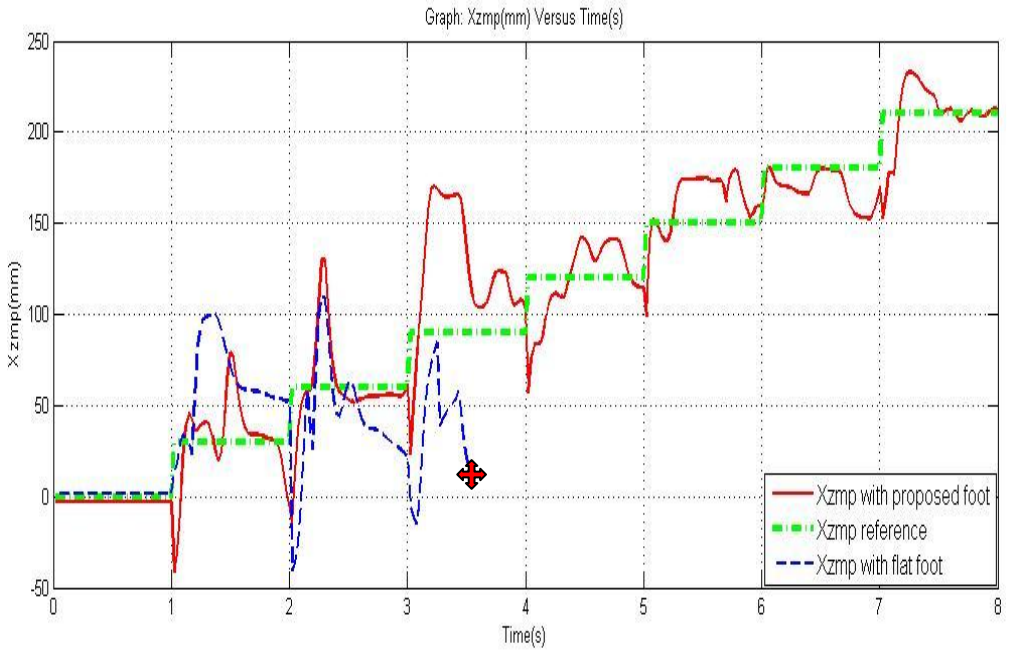

Figure 6.12: The variation of Xzmp(mm) when the robot is walking on the slope with gradient of 7 degree (with and without the proposed foot)

Figure 6.12 and 6.13 show the variation of Xzmp and Yzmp respectively when the robot was walking on the raised platform for three consecutive walking cycles. Based on the graph above, the Xzmp and Yzmp of the bipedal robot with the proposed foot were maintained near to the ZMP reference. The bipedal robot required at most 0.6s to enter the steady state.

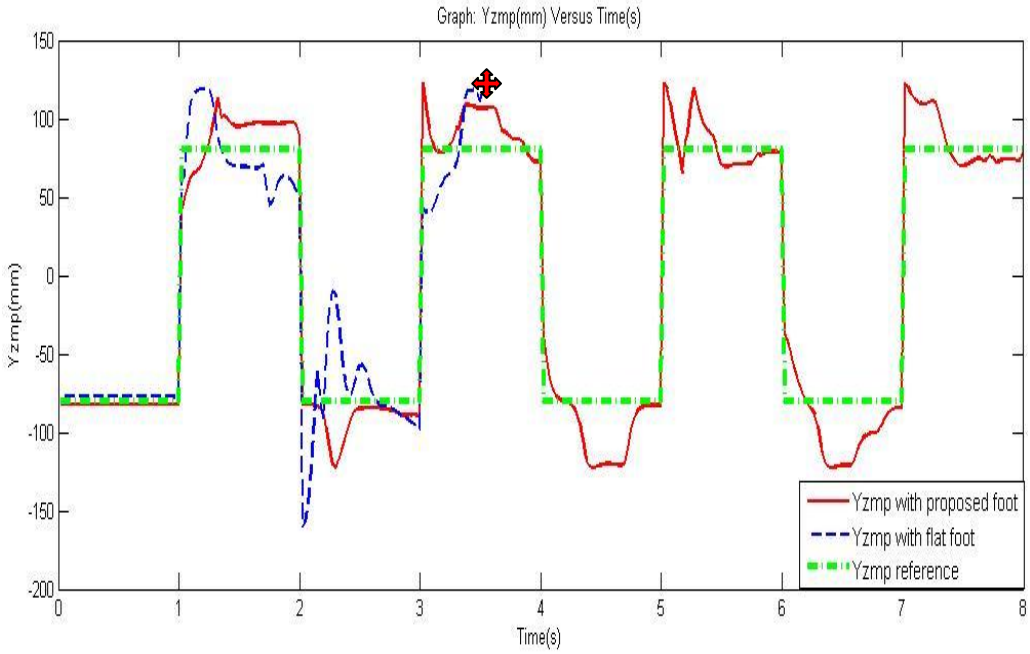

Figure 6.13: The variation of Yzmp(mm) when the robot is walking on the slope with gradient of 7 degree (with and without the proposed foot)

Besides moving in sagittal plane, the bipedal robot has to adapt to the raised platform along Z-axis and unevenness in lateral plane. Hence, more time (as compared to walking forward motion) are required to reach the steady state. During steady state, the Xzmp and Yzmp were maintained at the centre of the supporting ankle until the end of single support period of the swinging leg. The steady ZMP value implies that the walking motion was subjected to less 'vibration'. Also, during single support phase, the variation of ZMP is less for the case with the proposed foot. The robot started to step on the slope at the time of 3s. Hence, there was a big variation in Yzmp when the bipedal robot started to step on the slope. Since the cylinders would maintain their position after the leg was lifted up (adapted to the gradient of the slope), hence the subsequent steps registered less variation in ZMP when the robot was changing from double support phase to single support phase and vice versa.

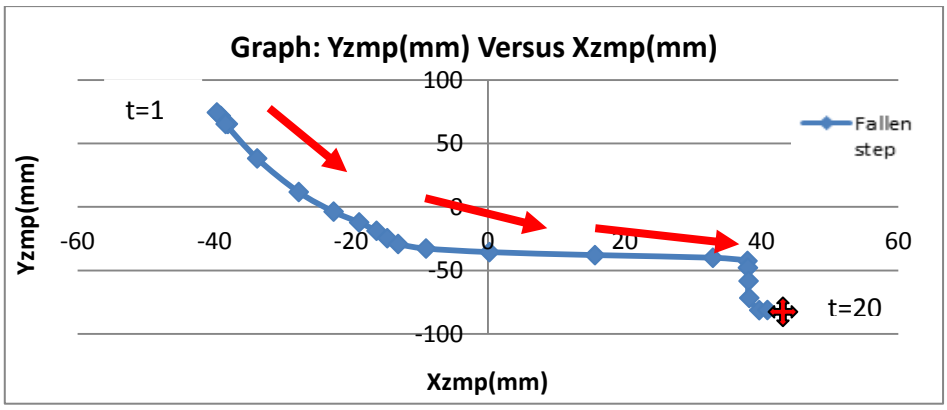

Figure 6.14: The variation of ZMP when the robot started to walk on a slope with gradient of 7 degree

For the case with flat foot, the robot fell backward at the time of 3.4s (marked as a cross in Figures 6.12 and 6.13 respectively). Figure 6.14 indicates the variation of ZMP for the falling step (on the left foot of the testing robot) when the robot was walking on the slope. The robot had fallen at the third step while it was trying to walk on the slope. The Red Cross (X) in Figure 6.14 indicates the time (at the sampling time of 20) when the robot fell down. The red arrow indicates the movement of ZMP on the left foot (the step that triggered falling). From the graph above, it is clear that the ZMP could not be maintained at the center of the ankle. Furthermore, it moved quickly from one edge to the other. Eventually, the robot fell backward. The variation of the ZMP (in closer view) on the proposed foot system is shown via Figure K and L in Appendix 1. Through these two figures, it is clear that the ZMP could be maintained near to the centre of the foot when the testing robot with the proposed foot was walking on the slope.

In order to quantify how well the ZMP fits to the reference ZMP, table 6.5 tabulates the mean SSE for Xzmp and Yzmp respectively. Based on table 6.5, the mean SSE for Xzmp and Yzmp are smaller for the case with the proposed foot. This implies that the ZMP for the case with the proposed foot are closer to the reference ZMP.

Table 6.5: Comparison of mean SSE for the case with and without the proposed foot during walking on a slope with gradient of 7 degree

Mean SSE	With Proposed Foot	Without Proposed Foot
Xzmp	0.02782	0.08918
Yzmp	0.03303	0.01696

Figure 6.15 shows the adaptability of the proposed foot on a slope with gradient of 7 degree.

Snapshots for Walking on a Slope with Gradient of 7 Degree

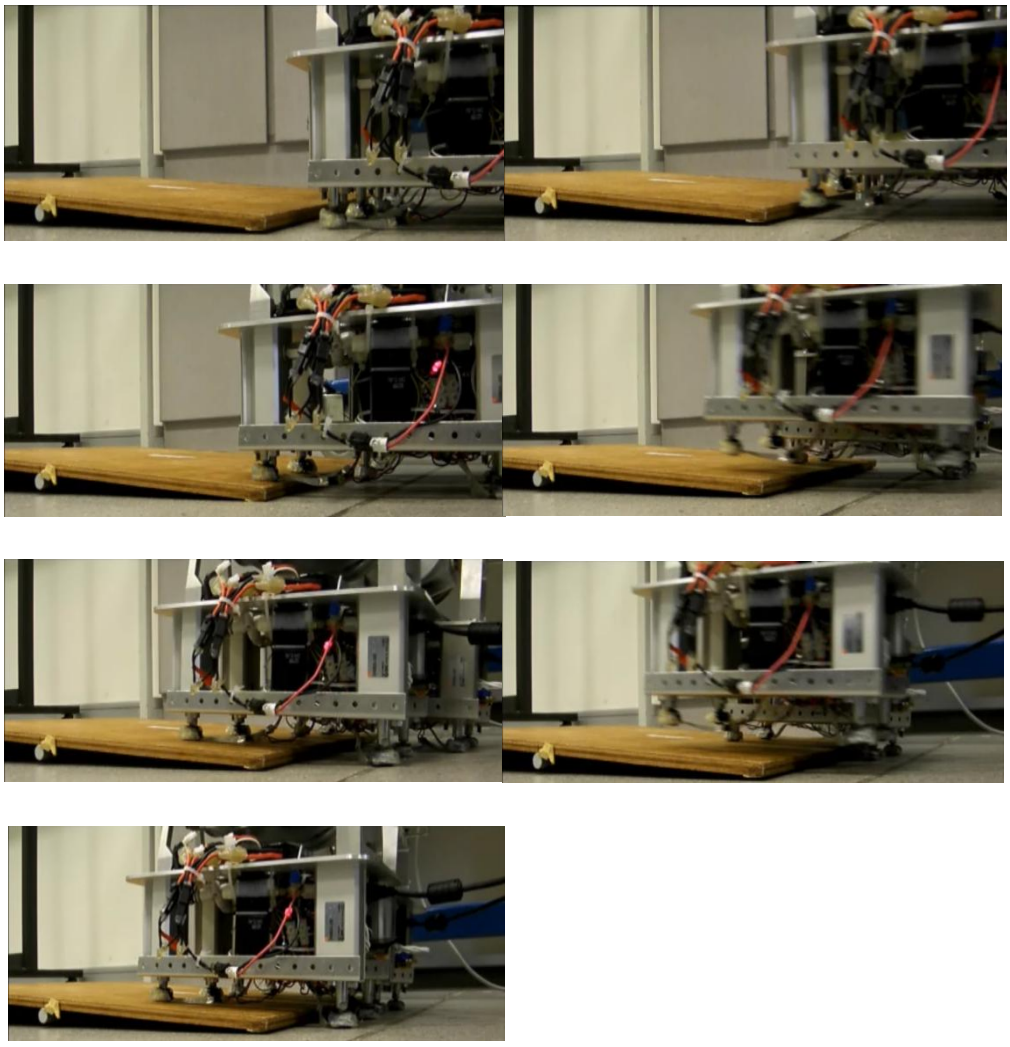

Figure 6.15: Snapshots for walking on a slope with gradient of 7 degree

6.3 Evaluation

Comparison the Proposed Foot System with Current Technology

This section compares the efficiency of the proposed foot system with current technology. The weight of the proposed foot system is 1.6 kg which is lighter than Waseda's shoes (1.85kg) [13]. Lighter foot is vital for fast swinging phase. The Waseda's Shoe (WS-1 & WS-1R) [16, 17] made used of four solenoids to achieve locking mechanism. On the other hand, the proposed foot system designed by the author merely made use of 3 solenoid valves to achieve the same objective. Hence, the proposed foot system is lighter than the Waseda's shoe. Besides, the Waseda's shoe made use of the mechanical micro switches to detect the landing state. The contact detection is not a direct measure which would further lengthen the delay for locking mechanism. For the proposed foot system, force sensing resistors are used to provide direct measurement of landing state. The rise time for FSR (1 to 2 millisecond) [5] is faster than the mechanical switch (0.01 second) [16, 17]. Hence, the locking mechanism can be triggered in more precise timing. Furthermore, the FSR can be used to estimate the position of ZMP in real time

The Waseda's Shoe (WS-1 & WS-1R) [16, 17] could only adapt to convex surface. For concave surface, the system would fail. This is because the system requires four contact points to be triggered at the same time. Some contacts points on the foot cannot reach the concave surface and subsequently the foot system cannot be locked. On the other hand, the extension and retraction of the hydraulic cylinders enables the proposed foot system to adapt concave surface. Kenji Hashimoto and Yusuke Sugahara [14] had come out with a new foot system design WS-5 (Waseda Shoes - No.5) to solve the problems of WS-1 & WS-1R. Equipped with new locking mechanism, the new Waseda's shoe is able to adapt to concave surface with 20 mm height. However, this new designed has made the foot system more complicated, bulkier and heavier which has a weight of 2.93kg. A heavy foot not only

decreases the walking motion stability but also decrease the swinging speed of the bipedal robot. Also, this new foot system is not rigid and robust which makes it difficult to walk continuously for a long time [14]. For the proposed foot system, it is lighter, robust and rigid for the testing robot to walk continuously.

Sano and Yamada have come out with a point-contact type foot with springs (PCFS) [41]. This foot system is used to achieve stabilization of contact states between foot and ground and unknown terrain landing. However, the maximum weight allowable for the testing robot was not mentioned. In order to achieve rubble walking for bipedal robot, Kenichi Tokuda and Takafumi Toda have designed a new foot sensor which is composed of a foot sensor and a rubbing mechanism [43]. Via the sensor feedback from the foot, these two mechanisms are used together to estimate the robustness and the shape of the foot contact surface. Nevertheless, this foot system is too heavy and bulky [43].

In short, the characteristics of the proposed foot system include light, compact, rigid, simple and rapidly become rigid after stable contact state is achieved.

6.4 Problems of the Proposed Foot, Solutions and Precautions

The walking cycle in this experiment was set to 1.0s. If the walking cycle is short, the hydraulic system may not have sufficient time to achieved steady state where the ZMP is maintained at the centre of supporting foot. Moreover, since the force sensing resistors (FSR) are attached at the tip of the hydraulic cylinders, the sensitivity of the FSRs would be decreased if they are subjected to high shear force. Then, the contacts points could not adapt to the fluctuation of the contact surface. The shear force is mainly due to slippage at the contact points. Hence, friction pads have to be installed to prevent slippage.

As mentioned in Chapter 2, the landing foot should be as flat as possible relative to the ground. As shown in Figure 6.16 below, if the landing foot is slanted with respect to the contact surface, the fluid exchange might be

hindered because there might not be sufficient normal force (landing impact normal to the contact point) to enable the fluid exchange among the cylinders.

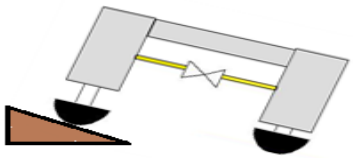

Figure 6.16: Failure condition (front view)

If the hydraulic system on the proposed foot system is not maintained at the pressures that the hydraulic cylinder could sustain during landing, an external leakage might be occurred. A small amount of hydraulic fluid leakage would facilitate air and dust particles from entering the hydraulic cylinder when it is retracting. The dust particles and the trapped air bubbles would result in internal contamination and rubbery action during cylinder rod movement. Contamination in solenoid valve and hydraulic cylinders could cause locking mechanism jamming and slow locking response. The hydraulic fluid selected must be kept in clean condition. Most of the hydraulic system failures are due to fluid contamination with water, dust and other foreign particle.

Generally, improper hydraulic system operation might due to insufficient fluid volume, trap of air bubbles in the system, foreign particles contamination, internal or external fluid leakage and inappropriate hydraulic fluid selection. In short, the selection of hydraulic cylinders, solenoid valve and hydraulic fluid must be carefully selected as discussed in Chapter 5.

Chapter 7: Conclusions

In order to achieve stable bipedal walking motion on rough terrain, it is necessary to stabilize the contact state between the foot and the ground. However, on rough terrain, the contact state is difficult to be maintained as the foot is easily separated from the contact surface for the bipedal robot with rigid and flat foot. Hence, a new foot system is proposed which has the following advantages which include stabilization of contact state, estimation of the ZMP position, absorption of landing impact and faster response in achieving stable state. This design is a complementary method that contributes to rough terrain walking motion. A new landing pattern with dorsiflexion and plantarflexion is proposed as well to work together with the proposed foot system. This landing pattern could increase the adaptability of the testing robot during walking motion on a raised platform. The design flow for the proposed foot system is presented.

Finally, the proposed foot system has been demonstrated to perform better than rigid flat foot for walking on uneven (moderate) terrain and also even terrain. The proposed foot system provides the absorption of landing impact, facilitates the establishment of stable contact state and the estimation of stable ZMP position during support phase.

Chapter 8: Recommendations

In this section, some recommendations will be discussed to increase the stability and robustness of the proposed foot.

8.1 Components Selection and Structure Design

In the proposed foot system, hydraulic cylinders are used as an actuator to adapt the fluctuations on the contact surface. However, this kind of hydraulic cylinder is relatively heavy (250g) and bigger in size if it is compared to a pneumatic cylinder (125g). Some researchers have justified that pneumatic cylinders can be used to replace hydraulic cylinders if the actuation power requirement is not very high and the fluid used is low in viscosity. In order to reduce the weight and size, pneumatic cylinders may be used to replace hydraulic cylinders.

Current foot design has four contact points. However, it is not easy to maintain four contact points simultaneously especially on the uneven terrain. A foot design with three contact points as shown in Figure 8.1 below might be sufficient.

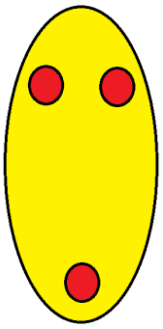

Figure 8.1: The layout of three contact points design

8.2 Sensor Fusion

Currently, the landing state detection is a passive system. The condition of the contact surface could be known only after the landing state. In the future, sonar sensor might be attached to the foot so that the landing ground conditions could be detected. The maximum fluctuation that can be tolerated by the proposed foot system is 20mm. If the sonar sensor detects a higher fluctuation, the bipedal robot should move the landing foot to another position before landing.

References

[1] A. Goswami. “Postural stability of biped robots and the foot-rotation indicator (FRI) point. *International Journal of Robotics Research*,” 18(6):523–33, June 1999.

[2] A.Takanishi, T.Takeya, H.Karaki, M.Kumeta and I.Kato, “A Control Method for Dynamic Walking under Unknown External Force,” In Proc. of the IEEE/RSJ IROS 1990, pp.795-801, Tsuchiura, Japan, July, 1990.

[3] F. Asano, M. Yamakita, N. Kamamichi and Z.W. Luo. “A novel gait generation for biped walking robots based on mechanical energy constraint,” In *Proc. of the IEEE/RSJ International Conference on Intelligent Robots and Systems*, pages 2637–44, 2002.

[4] H. J. Kang, S. Momoki, H. kondo, K. Hashimoto, H. O. Lim and A. Takanishi “Attitude Compensation Control for Biped Humanoid Robot”, the 12th International conference on CLimbing And Walking Robots and the support technologies for mobile machines, 2009.

[5] FSR 402 Data Sheet. Retrieved March 3, 2013, from http://www.sgbotic.com/products/datasheets/sensors/FSR402_datasheet.pdf

[6] J. H. Park, “Impedance Control for Biped Robot Locomotion,” IEEE Transactions on Robotics and Automation, Vol. 17, No. 6, pp. 870-882, 2001.

[7] J. H. Park and H. Chung, “ZMP Compensation by On-Line Trajectory Generation for Biped Robots,” in Proc. of the 1999 IEEE System, Man and Cybernetics, pp. 960-965, 1999.

[8] J. Perry. Gait Analysis: Normal and Pathological Function. Thorofare, NJ: Slack 1992.

[9] J. Rose and J. G. Gamble, ed. (1994). Human Walking, 2nd ed. Baltimore, Maryland: Williams & Wilkins.

[10] J. Yamaguchi, A. Takanishi and I. Kato, “Experimental Development of a Foot Mechanism with Shock Absorbing Material for Acquisition of Landing Surface Position Information and Stabilization of Dynamic Biped Walking,” Proc. of the IEEE International Conference on Robotics and Automation, pp. 2892-2899, 1995.

[11] J. Yamaguchi, N. Kinoshita, A. Takanishi and I. Kato, ”Development of a Biped Walking Robot Adapting to an Unknown Uneven Surface”, Journal of the Robotics Society of Japan, vol.14, no.4, pp.546-559, 1996 (in Japanese).

[12] J. Y. Kim, I. W. Park and J. H. Oh, ”Walking Control Algorithm of Biped Humanoid Robot on Uneven and Inclined Floor”, Journal of Intelligent and Robotic Systems, vol.48, no.4, pp. 457-484, April 2007.

[13] K. Hashimoto, Y. Sugahara, A. Hayashi, M. Kawase, T. Sawato, N. Endo, A. Ohta, C. Tanaka and A. Takanishi, "New Foot System Adaptable to Convex and Concave Surface," *Robotics and Automation, 2007 IEEE International Conference on* , vol., no., pp.1869-1874, 10-14 April 2007.

[14] K. Hashimoto, Y. Sugahara, A. Ohta, H. Sunazuka, C. Tanaka, M. Kawase, H. Lim and A. Takanishi , "Realization of Stable Biped Walking on Public Road with New Biped Foot System Adaptable to Uneven Terrain," *Biomedical Robotics and Biomechatronics, 2006. BioRob 2006. The First IEEE/RAS-EMBS International Conference on,* vol., no., pp.226-231, 20-22 Feb. 2006.

[15] K. Hashimoto, Y. Sugahara, H. O. Lim and A. Takanishi, “Biped Landing Pattern Modification Method and Walking Experiments in Outdoor Environment,” Journal of Robotics and Mechatronics, Vol. 20, No. 5, pp. 775-784, 2008.

[16] K. Hashimoto, Y. Sugahara, H. O. Lim and A. Takanishi, “Development of New Foot System Adaptable to Uneven Terrain for All Biped Robots,” Proc. of the 17th CISM-IFToMM Symposium on Robot Design, Dynamics and Control (ROMANSY2008), pp. 391-398, 2008.

[17] K. Hashimoto, Y. Sugahara, H. O. Lim and A. Takanishi, “New Biped Foot System Adaptable to Uneven Terrain,” Journal of Robotics and Mechatronics, Vol. 18, No. 3, pp. 271-277, 2006.

[18] K. Hirai, M. Hirose, Y. Haikawa and T. Takenaka, “The Development of Honda Humanoid Robot,” in Proc. of the 1998 IEEE International Conference on Robotics and Automation, pp. 1321-1326, 1998.

[19] K. Hirai, M. Hirose, Y. Haikawa, and T. Takenaka, “The Development of Honda Humanoid Robot,” Proc. of the IEEE ICRA 1998, pp. 1321- 1326, Leuven, Belgium, May, 1998.

[20] K. Kaneko, et al., “Design of Advanced Leg Module for Humanoid Robotics Project of METI,” Proc. of the IEEE ICRA 2002, pp. 38-45, Washington, DC, USA, May, 2002.

[21] K. Kaneko, F. Kanehiro, S. Kajita, H. Hirukawa, T. Kawasaki, M. Hirata, K. Akachi and T. Isozumi, ”Humanoid Robot HRP-2”, Proc. 2004 IEEE Int. Conf. on Robotics and automation, 2004.

[22] K. Nishiwaki, S. Kagami, J. Kuffner, M. Inaba and H. Inoue, “Humanoid ‘JSK-H7’: Reserch Platform for Autonomous Behavior and Whole Body Motion,” Proc. of the Third IARP International Workshop on Humanoid and Human Friendly Robotics, pp. 2-9, Tsukuba, Japan, December, 2002.

[23] K. Sabe, M. Fukuchi, J. S. Gutmann, T. Ohashi, K. Kawamoto and T. Yoshigahara, “Obstacle Avoidance and Path Planning for Humanoid Robots Using Stereo Vision,” Proc. of the 2004 IEEE International Conference on Robotics and Automation, pp. 592-597, 2004.

[24] L. Bloomfield, (2006). *How Things Work: The Physics of Everyday Life (Third Edition)*. John Wiley & Sons. pp. 153. ISBN 0-471-46886-X.

[25] M. Hirose, Y. Haikawa, T. Takenaka and K. Hirai, “Development of Humanoid Robot ASIMO,” Proc. of the IEEE/RSJ IROS 2001, Workshop2, Maui, Hawaii, USA, 2001.

[26] M. Morisawa et al., “A Biped Pattern Generation Allowing Immediate Modification of Foot Placement in Real-time,” Proc. of IEEE International Conference on Humanoid Robots, pp.581-5862, 2006.

[27] M. Vukobratovic, B. Borovac, D. Surla and D. Stokic, *Biped Locomotion: Dynamics, Stability, Control and Applications*, Springer Verlag, Berlin, 1990.

[28] M. Vukobratovic and Yu. Stepanenko, “On the Stability of Anthropomorphic Systems,” Mathematical Biosciences, vol. 15, no. 1, pp. 1-37, 1972.

[29] M. Yagi and V. J. Lumelsky, “Biped Robot Locomotion in Scenes with Unknown Obstacles,” Proc. of the 1999 IEEE International Conference on Robotics and Automation, pp. 375-380, 1999.

[30] M. Yamada, H. Maie, Y. Maeno, S. Sano and N. Uchiyama , "Design of point-contact type foot with springs for biped robot," *Advanced Intelligent Mechatronics (AIM), 2010 IEEE/ASME International Conference on* , vol., no., pp.806-811, 6-9 July 2010

[31] N.R. Draper and H. Smith, ed. (1998). *Applied Regression Analysis* (3rd ed.). John Wiley

[32] P. Michel, J. Chestnutt, S. Kagami, K. Nishiwaki, J. Kuffner and T. Kanade, “GPU-accelerated Real-Time 3D Tracking for Humanoid Locomotion and Stair Climbing,” Proc. of the IEEE/RSJ IROS 2007, pp. 463-469, 2007.

[33] P. Michel, J. Chestnutt, S. Kagami, K. Nishiwaki, J. Kuffner and T. Kanade, “Online Environment Reconstruction for Biped Navigation,” Proc. Of the 2006 IEEE International Conference on Robotics and Automation, pp. 3089-3094, 2006.

[34] P. Sardain and G. Bessonnet, "Forces acting on a biped robot. Center of pressure-zero moment point," *Systems, Man and Cybernetics, Part A: Systems and Humans, IEEE Transactions on*, vol.34, no.5, pp. 630- 637, Sept. 2004

[35] P. Sardain and G. Bessonnet, “Gait analysis of a human walker wearing robot feet as shoes,” In Proc. of the 2001 IEEE International Conference on Robotics and Automation, Seoul, Korea, pages 2285–92, May 2001.

[36] Q. Huang, Y. Nakamura and T. Inamura, “Humanoids Walk with Feedforward Dynamic Pattern and Feedback Sensory Reflection,” in Proc. of 2001 IEEE International Conference on Robotics and Automation, pp. 4220-4225, 2001.

[37] S. Cuccurullo, “Physical Medicine and Rehabilitation Board Review,” New York: Demos Medical Publishing, 2004.

[38] S. Kagami, et al., “Online 3D Vision, Motion Planning and Bipedal Locomotion Control Coupling System of Humanoid Robot: H7,” Proc. of the IEEE/RSJ IROS 2002, pp. 2557-2562, Lausanne, Switzerland, October, 2002.

[39] S. Kajita, F. Kanehiro, K. Kaneko, K. Yokoi and H. Hirukawa, “The 3D Linear Inverted Pendulum Mode: A simple modeling for a biped walking pattern generation,” Proc. of the IEEE IROS 2001, pp. 239- 246, Maui, Hawaii, USA, November, 2001.

[40] S. Kajita, K. Yokoi, M. Saigo and K. Tanie, “Balancing a Humanoid Robot Using Backdrive Concerned Torque Control and Direct Angular Momentum Feedback,” Proc. of the IEEE ICRA 2001, pp. 3376-3382, Seoul, Korea, May, 2001.

[41] S. Sano, M. Yamada, N. Uchiyama and S. Takagi, ”Point-Contact Type Foot with Springs and Posture Control for Biped Walking on Rough Terrain”, Proc. the 10th IEEE Int. Workshop on Advanced Motion Control, vol.2, pp.480-485, 2008.

[42] S. William and Levine, ed. (1996). *The Control Handbook*. New York: CRC Press.

[43] T. Koji, Tokuda, K. Toda, Y. Konyo, M.Tadokoro and S.Alain, "Estimation of fragile ground by foot pressure sensor of legged robot," *Advanced Intelligent Mechatronics, 2003. AIM 2003. Proceedings. 2003 IEEE/ASME International Conference on*, vol.1, no., pp. 447- 453 vol.1, 20-24 July 2003

[44] T. Sugihara and Y. Nakamura, "Whole-body Cooperative Balancing of Humanoid Robot using COG Jacobian," Proc. of the 2002 IEEE/RSJ International Conference on Intelligent Robots and Systems, pp.2575-2580, 2002.

[45] Y. Hurmuzlu and D. B. Marghitu, "Rigid body collisions of planar kinematic chains with multiple contact points," *International Journal of Robotics Research*, 13(1):82–92, 1994.

[46] Y. Ogura, H. Aikawa, Hun-ok Lim and A. Takanishi, "Developed of a human-like walking robot having two 7-DOF legs and a 2-DOF waist," Proc. of the IEEE international conference on robotics and automation, pp. 134-139, 2004.

[47] Y. Ogura, K. Shimomura, Hun-ok Lim and A. Takanishi, "Human-like Walking with Knee Stretched, Heel-contact and Toe-off Motion by a Humanoid Robot," Proc. of the IEEE/RSJ international conference on intelligent robots and systems, pp. 2497-2502, 2006.

[48] Y. Okumura, T. Tawara, K. Endo, T. Furuta and M. Shimizu, "Realtime ZMP Compensation for Biped Walking Robot using Adaptive Inertia Force Control," Proc. of the IEEE/RSJ IROS 2003, pp. 335-339, Las Vegas, USA, October, 2003.

[49] Y. Sugahara, T. Endo, H. O. Lim and A. Takanishi, "Design of a Battery-powered Multi-purpose Bipedal Locomotor with Parallel Mechanism," Proc. of the IEEE/RSJ IROS 2002, pp. 2658-2663, Lausanne, Switzerland, October, 2002.

[50] Y. Sugahara, T. Hosobata, Y. Mikuriya, H.O. Lim and A. Takanishi, "Realization of Stable Dynamic Walking by a Parallel Bipedal Locomotor on Uneven Terrain Using a Virtual Compliance Control," Proc. of the IEEE/RSJ IROS 2003, pp. 595-600, Las Vegas, USA, October, 2003.

[51] S. Butterworth, "On the Theory of Filter Amplifiers" In Wireless Engineer, vol. 7, 1930, pp. 536–541.

Appendices

I. ZMP Trajectory on Foot Plate

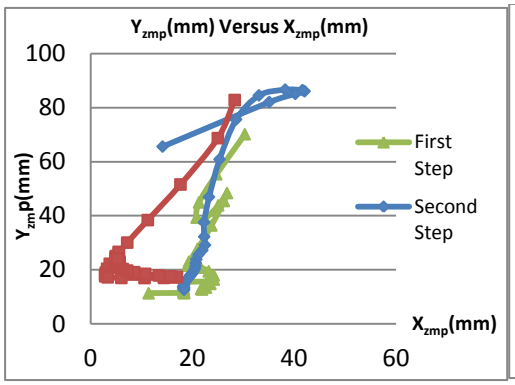

Figure A

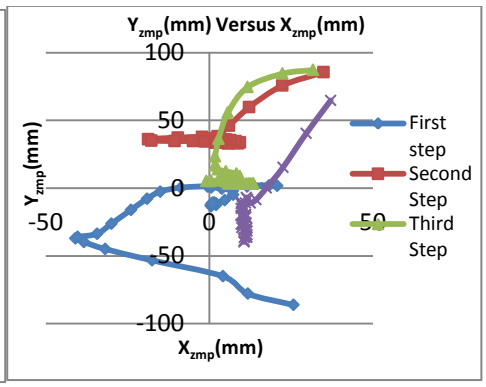

Figure B

Figure A and B show the ZMP(X versus Y) for left and right foot respectively when the bipedal robot was walking on the spot for three consecutive cycles with the proposed foot system. The ZMP for right and left foot were maintained close to the centre of the foot during the steady state. The overlapping portion indicates the steady state of single support phase.

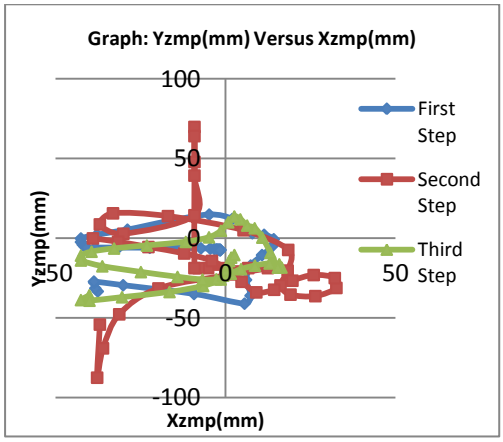

Figure C

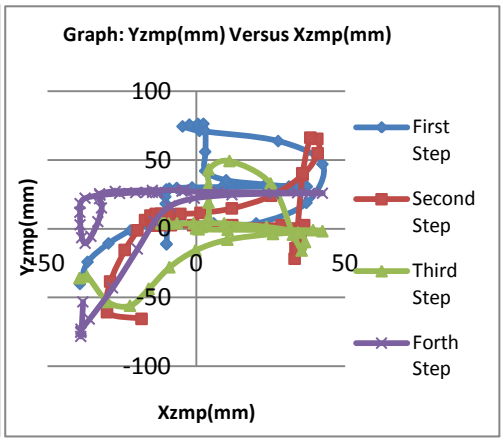

Figure D

Figure C and D show the ZMP(X versus Y) variation for left foot and right foot respectively when the bipedal robot was walking on the spot for three consecutive steps without the proposed foot. As compared with the case with the proposed foot, although most of the time the ZMP is maintained at the support polygon, the variation of the ZMP is large.

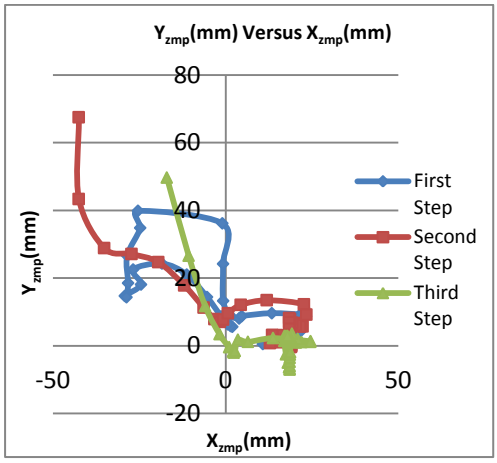

Figure E

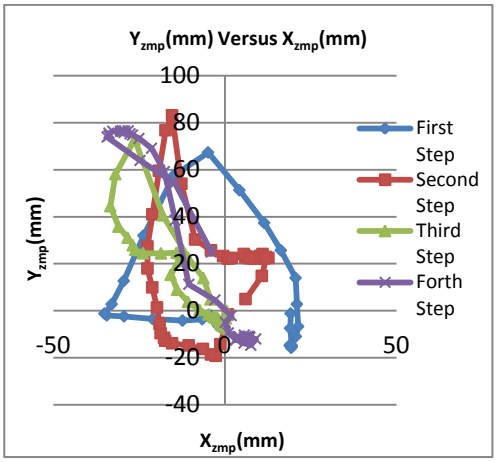

Figure F

Figure E and Figure F show the variation of ZMP recorded on left foot and right foot respectively while the bipedal robot was walking forward (3cm/step) with the proposed foot system. Similar to the case of on the spot motion, the ZMP for left and right foot were maintained near to the centre of the foot during steady state.

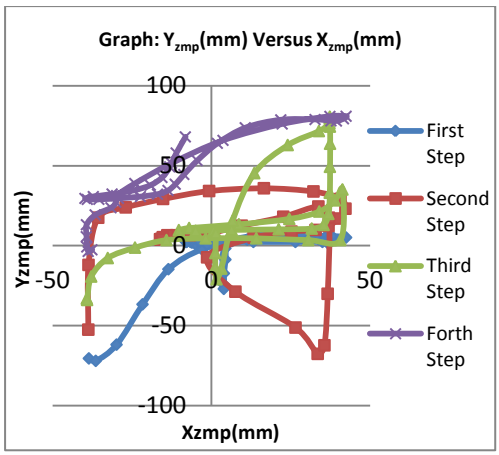

Figure G

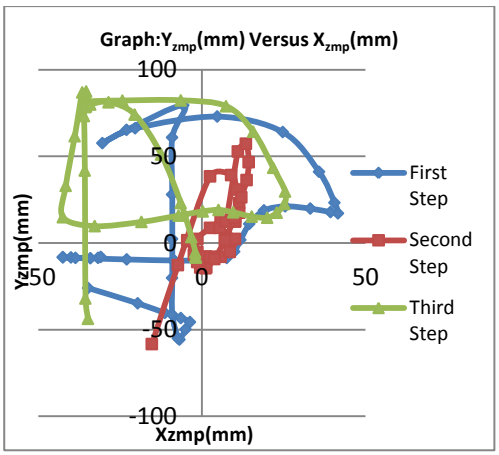

Figure H

Figure G and H show the ZMP(X versus Y) variation for left foot and right foot respectively when the bipedal robot was walking forward (2cm/step) for three consecutive walking cycles without the proposed foot. As compared with the case with the proposed foot system, although most of the time the ZMP is maintained at the support polygon, the variation of the ZMP is larger. Also, the steady state of ZMP could not be identified in this case.

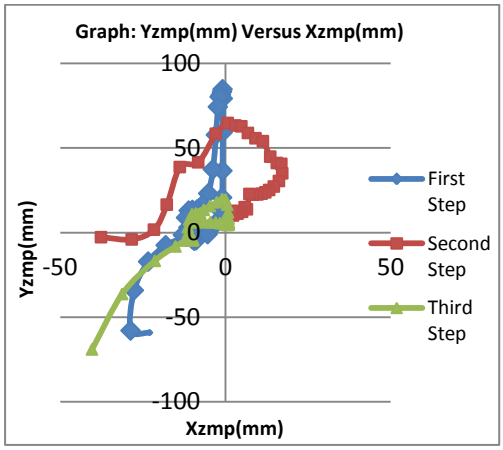

Figure I

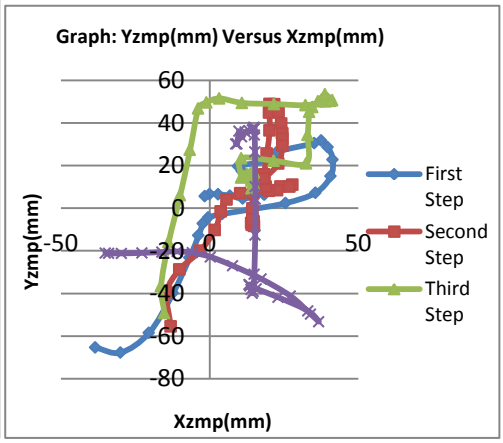

Figure J

Equipped with the proposed foot system, Figure I and J show the variation of ZMP recorded on left foot and right foot respectively while the bipedal robot was walking on a raised platform with a height of 1cm. Similar to the case of

walking forward motion, the ZMP for left and right foot were maintained near to the centre of the foot during steady state.

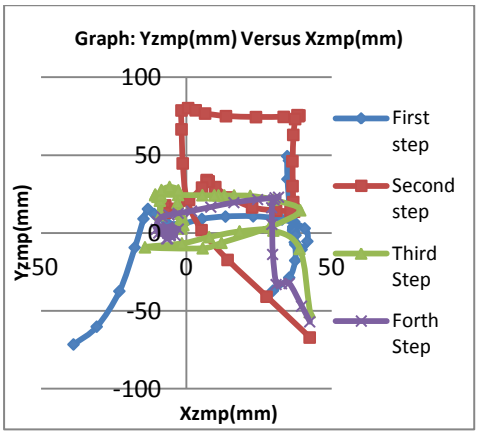

Figure K

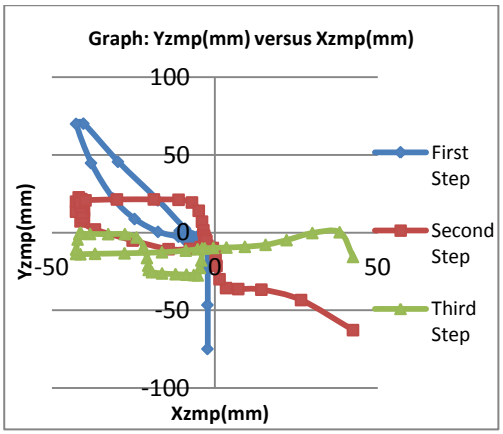

Figure L

Figure K and L show the variation of ZMP for left and right foot respectively when the bipedal robot with the proposed foot system was walking on the slope of 7 degree gradient. The ZMP could be maintained near to the centre of the foot which is important to form a firm foundation for supporting leg.

II. SSE Comparison

The summary of SSE for each step during different walking motion is tabulated in the tables below.

SSE for on the spot Motion

Table 1: SSE for Xzmp

SSE	1	2	3	4	5	6	7
without	0.06273	0.01114	0.02702	0.04526	0.01893	0.01627	0.04778
with	0.03092	0.00823	0.01213	0.020901	0.016612	0.01187	0.02885

Table 2: SSE for Yzmp

SSE	1	2	3	4	5	6	7
without	0.01988	0.02400	0.02265	0.02012	0.01644	0.01683	0.03371
with	0.01129	0.01802	0.00326	0.01964	0.00401	0.00409	0.00735

SSE for walking forward

Table 3: SSE for Xzmp

SSE	1	2	3	4	5	6	7
without	0.017655	0.055505	0.024984	0.021787	0.051167	0.12062	0.100444
with	0.016878	0.011335	0.018005	0.004842	0.029693	0.010628	0.084943

Table 4: SSE for Yzmp

SSE	1	2	3	4	5	6	7
without	0.036544	0.058541	0.09362	0.059002	0.068986	0.056373	0.043287
with	0.019801	0.024106	0.025521	0.002708	0.030233	0.028284	0.032765

SSE for walking on a raised platform

- The black region indicates the fallen state.

Table 5: SSE for Xzmp

SSE	1	2	3	4	5	6	7
without	0.151278	0.055677	0.280140				
with	0.021648	0.049119	0.024817	0.042349	0.043231	0.007165	0.036308

Table 6: SSE for Yzmp

SSE	1	2	3	4	5	6	7
without	0.013806	0.132806	0.061927				
with	0.011026	0.004851	0.013452	0.005901	0.0188	0.004873	0.014254

SSE for walking on slope

Table 7: SSE for Xzmp

SSE	1	2	3	4	5	6	7
without	0.061657	0.054461	0.151435				
with	0.021699	0.024021	0.094305	0.017474	0.016179	0.008546	0.012515

Table 8: SSE for Yzmp

SSE	1	2	3	4	5	6	7
without	0.020939	0.039981	0.038183				
with	0.013449	0.0092931	0.013314	0.028312	0.010483	0.029596	0.014239